

# Brain orchestration of pregnancy and maternal behavior in mice

David André Barrière<sup>1,2#</sup>, Arsène Ella<sup>1,3</sup>, Frédéric Szeremeta<sup>4</sup>, Hans Adriaensen<sup>1</sup>, William  
Même<sup>4</sup>, Elodie Chaillou<sup>1</sup>, Martine Migaud<sup>1</sup>, Sandra Même<sup>4</sup>, Frédéric Lévy<sup>1</sup>,  
Matthieu Keller<sup>1,#</sup>

<sup>1</sup> *Physiologie de la Reproduction et des Comportements, UMR INRAE/CNRS/Université de  
Tours/IFCE, Nouzilly, France.*

<sup>2</sup> *Université Paris-Saclay, CEA, CNRS, BAOBAB, NeuroSpin, 91191, Gif-Sur-Yvette, France.*

<sup>3</sup> *MRC Cognition and Brain Sciences Unit, University of Cambridge, UK.*

<sup>4</sup> *Complexes Métalliques et IRM, Centre de Biophysique Moléculaire, UPR 44301 CNRS,  
Orléans, France.*

**#Corresponding authors:**

[matthieu.keller@inrae.fr](mailto:matthieu.keller@inrae.fr) and [david.a.barriere@gmail.com](mailto:david.a.barriere@gmail.com)

17 **Abstract**

18 Reproduction induces changes within brain to prepare for gestation and motherhood. However,  
19 the dynamic of these central changes and their relationships with the development of maternal  
20 behavior remain poorly understood. Here, we describe a longitudinal morphometric  
21 neuroimaging study in female mice between pre-gestation and weaning, using new magnetic  
22 resonance imaging (MRI) resources comprising a high-resolution brain template, its associated  
23 tissue priors (60- $\mu$ m isotropic resolution) and a corresponding mouse brain atlas (1320 regions  
24 of interest). Using these tools, we observed transient hypertrophies not only within key regions  
25 controlling gestation and maternal behavior (medial preoptic area, bed nucleus of the *stria*  
26 *terminalis*), but also in the amygdala, caudate nucleus and hippocampus. Additionally, unlike  
27 females exhibiting lower levels of maternal care, highly maternal females developed transient  
28 hypertrophies in somatosensory, entorhinal and retrosplenial cortices among other regions.  
29 Therefore, coordinated and transient brain modifications associated with maternal performance  
30 occurred during gestation and lactation.

31

32 **Key words:** Gestation, lactation, maternal brain, MRI, atlas, voxel-based morphometry.

33 **Abbreviations:**

34 AC-PC: anterior commissure-posterior commissure

35 AMBMC: Australian Mouse Brain Mapping Consortium

36 AOB: accessory olfactory bulb

37 BNST: bed nucleus of the *stria terminalis*

38 CNS: central nervous system

39 CSF: cerebrospinal fluid

40 DARTEL: diffeomorphic anatomical registration using exponentiated lie algebra

41 df: degree of freedom

42 FA: flip angle

43 FLASE: fast large-angle spin-echo

44 FoV: field of view

45 MRI: magnetic resonance imaging

46 MOB: main olfactory bulb

47 mPOA: medial preoptic area

48 GM: gray matter

49 GMC: gray matter concentration

50 PVN: paraventricular nucleus of the hypothalamus

51 RARE: rapid acquisition with relaxation enhancement

52 ROC: receiver operating characteristic

53 ROI: region of interest

54 TE: echo time

55 TR: repetition time

56 VBM: voxel-based morphometry

57 WM: white matter

## 58 **Introduction**

59           Motherhood is among the most transformative experiences in the lives of female  
60 mammals. While virgin females tend to avoid neonates, the end of the gestation period and the  
61 birth process lead to a behavioral switch characterized by an attraction towards infant cues, the  
62 expression of nurturing behavior and ultimately the establishment of infant bonding<sup>1,2</sup>. Decades  
63 of scientific research dedicated to the maternal brain have revealed a core neural circuitry that  
64 includes the medial preoptic area (mPOA) and the adjoining ventral part of the bed nucleus of  
65 the *stria terminalis* (BNST<sub>v</sub>), and that is highly critical for the onset of maternal behavior<sup>1,3-5</sup>.  
66 Functional modulations of the mPOA/BNST<sub>v</sub> consistently disrupt maternal motivation and  
67 expression in numerous species<sup>1,2,6</sup>. This core maternal circuitry regulates maternal behavior  
68 through its direct projections to the ventral tegmental area, which promotes reward system  
69 activation<sup>1,7</sup>, as well as through its connections with cortical regions, including the prefrontal  
70 cortex<sup>8-10</sup>. This crucial central circuitry is finely regulated by multiple neural networks that  
71 integrate both internal and external stimulations. The proper expression of maternal care  
72 towards offspring is prepared through the neuroendocrine action of sex steroids and  
73 neuropeptides such as oxytocin among others during the gestation period<sup>11</sup>. These internal  
74 factors induce rewiring of the maternal brain, including through structural plasticity through  
75 increasing neuronal soma size or astrocytic complexity within the mPOA<sup>12</sup>, and changes in  
76 neurogenesis mainly in the main olfactory bulb (MOB)<sup>13</sup> but also in the mPOA/BNST in  
77 rodents<sup>14</sup>. In human, regional morphological changes of gray matter (GM) within the  
78 parahippocampal gyrus, precuneus, cingulate, insula and frontal cortex have been observed in  
79 primiparous women using magnetic resonance imaging (MRI)<sup>15</sup>. Additionally, olfactory cues  
80 coming from the neonate are integrated by the olfactory system within the MOB and the  
81 accessory olfactory bulb (AOB) through an amygdalo-hypothalamic pathway, which is  
82 responsible for attraction/repulsion behavioral outcomes<sup>16</sup>. Hence, the development of the

83 maternal brain is dependent of the integration of both external and internal cues acting through  
84 multiple brain pathways and regions to prepare the brain to gestation and motherhood.  
85 Nevertheless, the relationship between the brain rewiring over the gestation and lactation  
86 periods and the establishment of the maternal behaviors are poorly documented.

87 To assess the dynamics of the maternal brain, a longitudinal MRI morphometric study  
88 over a complete reproductive experience was performed in mouse to investigate changes in the  
89 gray matter concentration (GMC) using voxel-based morphometry (VBM). VBM is a well-  
90 established and well-validated image analysis technique that provides an unbiased and  
91 comprehensive assessment of anatomical differences throughout the brain, and has been  
92 successfully used to study GM changes within the mouse brain<sup>17-21</sup>. However, available mouse  
93 brain MRI resources are often partial or provided in different spatial orientations or spatial  
94 resolutions (**Table 1**). As an example, the [Australian Mouse Brain Mapping Consortium](#)  
95 (AMBMC), offers a high resolute template and a detailed atlases of the mouse brain including  
96 the cerebellum<sup>22</sup>, hippocampus<sup>23</sup>, diencephalon<sup>24</sup> and cortices<sup>25</sup>. Unfortunately, segmentation  
97 of the olfactory bulb and hindbrain is lacking, and this resource does not provide associated  
98 tissues probabilistic maps necessary for VBM. In other hand, the [Allen Mouse Brain Common](#)  
99 [Coordinate Framework](#), is the most advanced mouse brain atlas<sup>26</sup>. This new atlas delimitates  
100 discrete structures within the thalamus, hindbrain, olfactory system and diencephalon and  
101 provides a full segmentation of cortical layers however, MRI template and brain tissues priors  
102 are still lacking for VBM investigations.

103 Thus, we combined these resources and we associated probabilistic maps to emulate a  
104 complete resource dedicated to the mouse brain. Using these resources and a longitudinal VBM  
105 approach, we were able to assess the dynamic morphological changes of the brain during the  
106 whole reproductive period and demonstrate how these changes predicts the quality of maternal  
107 behavior.

## 108 **Results**

### 109 **Mouse MRI atlas**

110 VBM strategies require a template image and its associated priors of gray matter (GM),  
111 white matter (WM) and cerebrospinal fluid (CSF) for brain segmentation and normalization. In  
112 addition, a complete atlas of the mouse brain is mandatory for the identification of regions of  
113 interest (ROIs) highlighted by the VBM analysis. Given the limitations of available tools to  
114 thoroughly study GMC changes during the gestation and lactation periods in mice, we  
115 developed first a new set of resources using the AMBMC, an ultra-high-resolution template  
116 built from *ex vivo* brain images finely normalized within the same space<sup>25</sup> and the [Allen Mouse](#)  
117 [Brain Common Coordinate Framework](#)<sup>26</sup> (**Figure 1**). Our resources comprise the following four  
118 components: 1) a complete mouse brain template with a spatial resolution suitable for mouse  
119 brain analysis (60- $\mu$ m isotropic resolution); 2) the corresponding GM, WM and CSF  
120 probabilistic maps for brain normalization together with a VBM analysis built from 138 T<sub>2</sub>-  
121 weighted images; 3) a complete mouse brain atlas derived from Paxinos and Franklin's mouse  
122 brain atlas<sup>27</sup> and composed of a mosaic of 1320 ROIs (**Figure 2A**); 4) a brain mesh permitting  
123 brain plot generation and data visualization (**Figure 2B** and **Supplemental Video 1**). We  
124 visually inspected and carefully checked the results of the normalization process against the  
125 original coregistered atlas. Then, the labeled structures were reclassified and aggregated  
126 according to the brain regions to which they belonged (auditory, insular, temporal cortices,  
127 etc.), with respect to their anatomical topography (cortex, basal ganglia, etc.), tissue type (GM,  
128 WM and CSF) and hemisphere (left or right). Cortical structures were subdivided into  
129 functional (*e.g.*, primary and secondary motor cortices) or structural (agranular, dysgranular,  
130 agranular/dysgranular, granular and posterior agranular insular cortices) areas (**Figure 2C**), as  
131 well as into different cortical layers (**Figure 2D**). Subcortical structures, as for example, the

132 hypothalamus (**Figure 2E**) and the hippocampus (**Figure 2F**), were fully segmented according  
133 to Paxinos and Franklin's atlas<sup>27</sup>.

134

### 135 **Morphometric changes occurred during the gestation and lactation periods**

136         Next, we used our new resources to study the variations of GMC in mouse brain from  
137 the beginning of gestation until weaning. Using MRI T<sub>2</sub>-weighted anatomical acquisitions, we  
138 estimated the GMC maps that offer for each animal a global estimation of the GM. Longitudinal  
139 comparison of GMC between the control and parous groups permits to highlight local  
140 modifications of GM during the experience. A comparison of baseline and early gestation GMC  
141 maps between the control and parous groups did not reveal significant differences. However, at  
142 the end of the gestation period, significant increases in GMC were observed within several brain  
143 regions in the parous group compared to the control group (**Table S1** and **Figure 3A**). Time  
144 course analysis revealed differences in GMC profiles between control and parous groups at the  
145 end of the gestation period, early in lactation and at the end of the lactation period. Specifically,  
146 GMCs within the mPOA and the BNST were consistently significantly higher in the parous  
147 group at that times. In addition, within the agranular insular cortex in the late gestation period  
148 and the early lactation period, GMC was significantly higher in parous group compare to control  
149 group (**Figure 4A**). During the early lactation period, we also found specific and significant  
150 increases in GMCs of the parous group within numerous brain regions (**Table S2** and **Figure**  
151 **3B**). Among these structures, the hippocampus (CA1 layer), amygdalar area and piriform area  
152 showed a transient increase in GMC at the early lactation time point that returned to baseline  
153 values at the end of the lactation period in parous group compared to control group (**Figure**  
154 **4B**). In contrast, the caudate putamen, arcuate nucleus and paraventricular nucleus of the  
155 hypothalamus (PVN) showed significantly higher GMCs in the parous mice than in the control  
156 mice during the lactation period (**Table S3** and **Figures 3C and 4C**). Together, our data

157 demonstrate that the late gestation period is associated with a pronounced increase in GMC in  
158 the mPOA/BNST, the core neural system of maternal motivation, lasting up to the late lactation  
159 period. Furthermore, the early lactation period is associated with increased GMC in other key  
160 maternal motivation areas in midbrain regions, including the hypothalamus, caudate putamen  
161 and amygdala. These GMC differences between both groups were no longer observed after  
162 weaning.

163

### 164 **Morphometric changes during gestation predict the quality of maternal behavior**

165 In the last part of this work, we evaluated whether these morphometric changes might  
166 reflect differences in maternal performance. Based on 15 min of behavioral observation during  
167 the pup retrieval test performed one week after birth, we evaluated the maternal performance  
168 of each mother by measuring the first, second and third pup retrieval times, pup-licking  
169 duration, crouching time, rearing time, digging time and self-grooming time (**Figure 5A**).  
170 Interestingly, we observed a large distribution of values for both crouching (284.2 s,  $SD \pm 268.7$   
171 s) and digging (98.22 s,  $SD \pm 159.3$  s) durations within the parous group. Whereas crouching  
172 duration relates to maternal behavior, digging duration is widely recognized as a discriminative  
173 marker of stress-related behavior in rodents<sup>28</sup>. Hence, we used crouching and digging durations  
174 to cluster animals using the k-means clustering procedure, thereby clustering parous animals  
175 into a high maternal behavior group (those with a high crouching time and low digging time)  
176 and a low maternal behavior group (those with low crouching time and high digging time).

177 A comparison of maternal performance parameters between the two clustered groups  
178 revealed significantly lower crouching and pup-licking times and a significantly higher digging  
179 time (**Figure 5B**) in the low maternal behavior group (n=6) than in the high maternal behavior  
180 group (n=6). Moreover, a comparison of GMC maps revealed both cortical and subcortical  
181 differences between the two clustered groups, mainly in the late gestation period (**Table S4** and

182 **Figure 5C)** but also during the early lactation period (**Table S5** and **Figure 5D**). Indeed,  
183 transient increases in GMCs within the entorhinal area, lateral part of the orbital area, accessory  
184 olfactory bulb (AOB), and medial preoptic nucleus that were observed at the end of pregnancy  
185 in the high maternal behavior group were absent in the low maternal behavior group (**Figure**  
186 **6A**). In addition, the high maternal behavior group showed consistent higher GMCs in the  
187 hippocampus, retrosplenial area and barrel field of the primary somatosensory cortex (**Figure**  
188 **6B**) from the end of the gestation until the end of the lactation period.

189           Interestingly, using a receiver operating characteristic (ROC) analysis, we found that  
190 GMCs values within the entorhinal area and AOB at late gestation are reliable predictors for  
191 mouse maternal performance after birth. These GMC values significantly distinguished low  
192 maternal performance from high maternal performance postpartum (entorhinal area: sensitivity  
193 = 100, confidence interval (CI) = 61% to 100%; specificity = 83, CI = 44% to 99%; likelihood  
194 ratio = 6; **Figure 7A**; AOB: sensitivity =100, CI = 61% to 100%; specificity = 83, CI = 44% to  
195 99%; likelihood ratio = 6, **Figure 7B**). The GMC values of both the entorhinal area and AOB  
196 observed at late gestation were also significantly correlated with maternal behavior (crouching  
197 and digging times). These results reveal that the GMC differences in olfactory (AOB and  
198 entorhinal cortex) and mnemonic (entorhinal area)-related brain regions occurring during the late  
199 gestation period significantly predicted the quality of maternal behavior.

## 200 **Discussion**

201           Using a new comprehensive neuroimaging resources dedicated to mouse brain, this  
202 longitudinal study reveals that pregnancy and lactation coincide with pronounced and transient  
203 cerebral changes. Transient increases in GMCs were observed in key regions controlling  
204 maternal behavior (mPOA, BNST, and PVN), as well as regions involved in emotions  
205 (amygdala), in motivation and reward (caudate nucleus, orbitofrontal cortex) and in mnemonic  
206 functions (hippocampus). Interestingly, increase in GMC was also revealed in the insular cortex  
207 thought to link social and emotional skills. Moreover, we showed that females expressing high  
208 levels of maternal behavior had developed specific increases in GMCs in structures involved in  
209 olfactory (MOB and AOB) and somatosensory (somatosensory cortex) information processing,  
210 in memory (hippocampus, entorhinal cortex, retrosplenial cortex) and in reward and  
211 reinforcement (striatum). Interestingly, these hypertrophies were already significant at the end  
212 of the gestation period thus being predictive of the quality of maternal care (**Supplemental**  
213 **Video 2**).

214

## 215 **Implementation of new resources to support the analysis of mouse brain MRI data**

216           The use of preclinical MRI is a target of growing interest for the study of the brain  
217 structure and function in both healthy and pathological conditions. The use of advanced MRI  
218 techniques, coupled with the development of advanced animal models, is a powerful way to  
219 push new breakthroughs in the understanding of brain functioning and pathology. Herein, in  
220 the first step in our study, from the recent major advances in the development of brain mouse  
221 atlas we generated a new set of neuroinformatic tools offering for the first time a complete  
222 resource dedicated to MRI studies of the mouse brain, namely, an accurate brain atlas (1320  
223 ROIs), a high-resolution brain template and the associated GM, WM and CSF priors (60- $\mu$ m  
224 isotropic resolution). The GM, WM and CSF probabilistic maps built and used in this study

225 were calculated from 138 T<sub>2</sub>-weighted anatomical images, resulting in robust tissue class priors  
226 not only for VBM analysis but also for functional MRI and diffusion tensor imaging analysis  
227 in mice.

228 This comprehensive set of MRI compatible template and atlas for the mouse brain,  
229 allows a unified and standardized analysis of multimodal mouse brain MRI data and paves the  
230 way for the development of multicentric preclinical studies. Indeed, in neurosciences, animal  
231 models deliver crucial information for the understanding of brain structure and function both in  
232 healthy and pathological conditions. Our template and mouse brain atlas were conceived to  
233 bridge the gap between basic and clinical neurosciences by providing to the preclinical  
234 neuroimaging community specific resources designed to be used in conjunction with the  
235 neuroinformatic tools and methodologies commonly used in human MRI studies. We anticipate  
236 that these resources will help neuroscientists to conduct their analyses of anatomical and  
237 functional datasets in a more standardized way, with the final goal of reaching more  
238 reproducible conclusions (<https://www.nitrc.org/projects/tmbta> 2019).

239

#### 240 **Gestation and lactation periods induce strong but transient GMC hypertrophy**

241 The establishment of accurate mouse MRI resources permit to study the variations of  
242 GMC longitudinally, *in vivo* and during the gestation and lactation periods in female mice. We  
243 observed that several brain regions became transiently hypertrophic during pregnancy or in the  
244 lactation period until weaning. A set of structures comprising the core of the maternal circuit –  
245 especially the mPOA and BNST – displayed long-lasting hypertrophy that started at the late  
246 gestation, culminated during the first week of lactation, and then disappeared at the weaning.  
247 The initial GMC increase observed during the gestation period probably reflects changes  
248 induced by hormonal priming<sup>11</sup>. Indeed, both the mPOA and BNST express a high number of  
249 steroid hormone and neuropeptide receptors<sup>29,30</sup>. These factors are well known to trigger

250 significant plasticity changes within the core maternal circuitry that are necessary for the  
251 preparation and adaptation of the brain to motherhood<sup>3,11</sup>. From parturition, the GMC  
252 differences observed during the whole lactation period highlight that mPOA/BNST receives a  
253 variety of sensory inputs from the pups, integrates that information with the females' endocrine  
254 status, and then projects to brain sites involved in socially-relevant motivation, affective state,  
255 and cognition<sup>2,31</sup>. Pup stimulation, electrolytic and neurotoxic lesions and local steroid hormone  
256 injections<sup>32-35</sup> have been shown to modify the intrinsic activity of these nuclei and consequently  
257 responsible for motivation and expression of maternal behavior. The mPOA is engaged  
258 throughout the postpartum period but differentially according to the needs of the developing  
259 pups. It has been shown that neurons of the mPOA in late postpartum inhibits maternal  
260 responses allowing the changing expression and waning of maternal behavior across  
261 postpartum<sup>10</sup>. The sustained increase in GMC reported in late lactation could reflect the  
262 involvement of the mPOA to appropriately influence maternal behavior.

263 Our study highlights another set of brain structure that became hypertrophic only during  
264 the period from parturition to weaning – specifically, the PVN and arcuate nucleus of the  
265 hypothalamus. These changes illustrate the structural plasticity occurring in these regions. For  
266 instance, at parturition and during lactation oxytocin neurons of the PVN undergo dramatic  
267 neuronal, glial and synaptic changes such as an increase in size of the oxytocin neurons and an  
268 amplification of their synaptic input<sup>36</sup>. Oxytocin release at parturition facilitates the onset of  
269 maternal behavior by acting on the mPOA and is also important for maternal memory<sup>37</sup>. Finally,  
270 lesions of the PVN disrupt the onset of maternal behavior<sup>38-40</sup>. In the arcuate nucleus,  
271 dopaminergic cells are responsible for suckling induced prolactin release<sup>41</sup>. and neurons  
272 projecting to the arcuate nucleus are involved in the maintenance of maternal motivation<sup>42</sup>.

273 Additionally, we report changes in GMCs found in olfactory related structures (main  
274 olfactory bulb, piriform cortex), somatosensory areas and auditory areas which reflect the

275 multisensory control of maternal behavior. This finding is in accordance with a functional MRI  
276 study performed in rats which demonstrates that pup suckling is associated with increased  
277 neuronal activity within the midbrain, striatum and cortical sensory areas (somatosensory,  
278 olfactory and auditory cortices)<sup>9</sup>.

279 GMC variations within the hippocampus and entorhinal cortex, highlight the role of two  
280 essential structures involved in learning and memory processing during the reproductive period.  
281 Our data support evidence that the hippocampus undergoes profound neural changes during  
282 lactation. Indeed, lactating females have elevated spine densities in the hippocampus<sup>43</sup> and  
283 show significant dendritic remodeling in pyramidal neurons<sup>44</sup>. Changes in hippocampal  
284 neurogenesis occurs during lactation and may support the enhancement of spatial memory  
285 necessary to foraging behavior in lactating females<sup>43,45</sup>.

286 Finally, our study also revealed an hypertrophy of the agranular insular cortex, which  
287 has never been reported in this context. The agranular insular cortex is a laminar part of the  
288 insular cortex and can be considered as a hub structure linking large-scale brain systems<sup>46</sup>.  
289 Indeed, the insula receives direct thalamic and somatosensory afferents carrying sensitive  
290 stimulations. In addition to its sensory afferents, the insula displays structural connectivity with  
291 the limbic system (basolateral, lateral and central amygdalar nuclei) as well as with the BNST,  
292 mediodorsal nucleus of the thalamus, lateral hypothalamus and perirhinal and lateral entorhinal  
293 cortices<sup>46</sup>. The insula also connects brain regions implicated in motivation and reward, such as  
294 the nucleus accumbens and caudate putamen<sup>46</sup>. Hence, our findings and the current literature  
295 suggest that before and after birth, the insular cortex may integrate and combine information  
296 from both external and internal stimulation and act as a relay between higher cortical and  
297 subcortical structures. Together, our results describe the dynamics of neurophysiological  
298 adaptation occurring in the brain from the early gestation period to weaning, thereby ensuring  
299 efficient maternal behavior and, by extension, the development of the offspring.

300 **GMC modification in the olfactory system at the end of the gestation predict the level of**  
301 **maternal behavior post-partum**

302 All of these transient modifications of the GMC within the brain of parous animals  
303 demonstrate that many structures are involved in the behavioral modifications occurring during  
304 pregnancy and motherhood. Hence, in the last part of this work, we sought to determine whether  
305 inter-individual variations in maternal behavior were associated with similar variations of  
306 GMC. Based on their behavioral performance in the pup retrieval test, we used a k-means  
307 clustering strategy to divide maternal female mice into two groups displaying high *versus* low  
308 levels of maternal behavior. This analysis revealed that several transient and several long-  
309 lasting increases in GMCs were observed in the high maternal behavior group that were absent  
310 in the low maternal behavior group. Brain regions showing significant differences included the  
311 olfactory bulbs, somatosensory system, limbic system, especially the orbitofrontal area, and  
312 mnesic system, including the retrosplenial cortex, hippocampus and entorhinal area. Some of  
313 these structures are directly responsive to pup stimulation, and the observed dynamics may have  
314 been induced by mother-offspring interactions. For example, higher GMC values in the  
315 somatosensory cortex and olfactory bulbs in the high maternal behavior group potentially  
316 reflected increased suckling duration and proximity between the mother and pups, respectively.

317 Strikingly, differences in GMCs were detected in the entorhinal area, orbitofrontal area,  
318 olfactory bulb, hippocampus, retrosplenial area and primary somatosensory area before  
319 parturition; these findings suggest that the maturation of these structures, probably through  
320 hormone-dependent plasticity mechanisms, is a key determinant of the intensity of maternal  
321 behavior expressed during the lactation period. Using a ROC procedure, we found that GMC  
322 values of the entorhinal area and accessory olfactory bulb (AOB) at the end of gestation were  
323 significantly predictive of maternal mouse behavior postpartum. Interestingly, previous studies  
324 reported in mice showed that during gestation an increase in cell proliferation in the

325 subventricular zone, the neurogenic niche which provides newly generated neurons within the  
326 olfactory bulb (for review see <sup>13</sup>). These adult-born olfactory neurons are fully responsive to  
327 pup odor exposure<sup>47</sup> and are in part involved in some components of maternal behavior<sup>48,49</sup>.

328 Hence, the correlations observed between GMC values in AOB at the late gestation time  
329 point and maternal behavior after birth suggest that impairments of such neurogenesis processes  
330 induce maladaptive neuroendocrine processing of the maternal brain at the end of the gestation  
331 period impacting directly the maternal behavior performance postpartum. Taken together, our  
332 data provide the first potential imaging-based predictive biomarkers of the quality of maternal  
333 behavior and suggest the key role of the maturation of the olfactory system at the end of the  
334 pregnancy in the development of adaptative maternal behavior in mice.

335

## 336 **Conclusion**

337 In conclusion, our study provides a new generation of neuroinformatic tools which will  
338 help basic neuroscientists to conduct structural and functional MRI investigations. Using these  
339 resources, we found that the development of the maternal brain is associated with substantial  
340 mesoscopic changes in critical regions. These modifications can be interpreted as cell size  
341 changes, neural or glial cell genesis/apoptosis, spine density or blood flow modifications<sup>50-52</sup>.  
342 As cellular and molecular plasticity events are key for the adaptation of the brain to motherhood;  
343 therefore, these changes in GMC must be correlated with molecular, cellular and behavioral  
344 investigations to obtain a more precise view of the physiological mechanisms responsible for  
345 GMC variations.

346 **Methods**

347 **Animals.** Twenty-three female RjOrl:SWISS virgin mice (8 weeks old; 20-25 g; Janvier  
348 Laboratory, Le Genest-Saint-Isle, France) were maintained on a 12-h light/dark cycle with  
349 access to food (standard chow) and water *ad libitum*. Animals were acclimatized 6 per cage to  
350 the housing facility for 7 days prior to manipulation. Females were randomly divided into two  
351 groups: a parous group (n = 12), in which each female was exposed to a male (RjOrl:SWISS,8  
352 weeks old; 20-25 g; Janvier Laboratory, Le Genest-Saint-Isle, France) for 5 days, became  
353 pregnant, and raised their offspring (litter size: 6 to 14 pups) until weaning at 21 days  
354 postpartum, and a control group (n = 11), in which virgin females were not exposed to male  
355 mice. Each parous female was individually housed after exposure and with its offspring  
356 postpartum. Control females were housed together in a separate room from parous females.

357 The MRI protocol was optimized to keep mice anesthetized for 2 h during each of the  
358 six acquisitions. During lactation MRI acquisitions, pups were kept under a heat lamp. One  
359 week after birth, maternal behavior was assessed as described in the behavioral section. All  
360 experiments were conducted in accordance with the local research ethics committee (APAFIS  
361 #6626-201002281145814V1) and are reported in accordance with the ARRIVE guidelines.

362

363 **MRI acquisition.** *In vivo* 3D MRI of the entire brain was performed three days before male  
364 exposure (baseline), at one week of gestation (early gestation), two days before the expected  
365 day of birth (late gestation), one week postpartum (early lactation), three weeks postpartum  
366 (late lactation) and two weeks after weaning (weaning). One female in the parous group and  
367 one female in the control group were scanned under similar conditions on the same day and  
368 exposed similarly to anesthesia.

369 Mice were anesthetized using isoflurane (2.5%; induction in O<sub>2</sub>/air mixture 1:1) (TEM-  
370 SEGA, F-33600 Pessac, France) and then transferred and placed head first *procurbitus* within

371 an MRI-compatible cradle that incorporated a stereotaxic system dedicated for mouse head  
372 MRI, connected to a heater with circulating water to maintain body temperature and supplied  
373 with 1-2% isoflurane *via* a fitted mask. Respiration rate was recorded during all the experiments  
374 using an MRI-compatible monitoring system (PC-SAM model #1025; SA Instruments Inc.,  
375 Stony Brook, NY, USA) and used to adjust the isoflurane rate to maintain a rate between 20  
376 and 40 respirations per minute. After a recovery period of one hour, mouse returned to her pups.  
377 MRI studies were conducted at the Centre de Biophysique Moléculaire d'Orléans and were  
378 performed on a 7T/160 mm PharmaScan spectrometer (Bruker Biospin, Wissembourg, France)  
379 equipped with an actively shielded B-GA09 gradient set, with 90-mm inner diameter and 300-  
380 mT/m gradient intensity. A 23-mm inner diameter Bruker birdcage coil with a cradle dedicated  
381 to a mouse head was used. Data acquisitions were performed on an Advance III console running  
382 ParaVision 5.1 software. T<sub>2</sub>-weighted images were acquired using a 3D fast large-angle spin-  
383 echo (FLASE) which allows 3D brain mapping with a high resolution in a suitable time for *in*  
384 *vivo* acquisition<sup>53,54</sup>. Thus, sequence with echo time (TE) = 20 ms, 1 repetition, acquisition  
385 matrix = 160 × 140 × 95, and a field of view (FoV) of 19.2 × 16.8 × 11.4 mm<sup>3</sup>, resulting in a  
386 final resolution of 120 μm isotropic voxels<sup>53,54</sup>. To obtain the FLASE sequence<sup>53</sup>, which is a  
387 specific sequence that is not included in the sequence package provided with ParaVision, the  
388 usual rapid acquisition with relaxation enhancement (RARE) spin-echo sequence was  
389 modified; in particular, the RARE-factor was fixed to 1 allowing a flip angle (FA) higher than  
390 90° for the excitation pulse, while maintaining a 180° refocusing pulse<sup>53</sup>. Thus, T<sub>2</sub>-weighted  
391 images were obtained with a repetition time (TR) as short as 300 ms, 10 times lower than that  
392 needed for a classical T<sub>2</sub>-weighted spin-echo sequence. The sequence was optimized for  
393 acquisition in 1 h 28 min, with an isotropic resolution of 120 μm, a TR of 300 ms, an TE of 20  
394 ms, an excitation pulse (FA) of 115°, with 1 repetition and with a matrix of 160 x 140 x 95  
395 corresponding to a FoV of 19.2 x 16.8 x 11.4 mm<sup>3</sup> and contained the whole mouse brain.

396 **Maternal behavioral test.** One week after birth, the maternal behavior of each female was  
397 evaluated using the pup retrieval test<sup>55</sup>. Briefly, three pups were removed from the nest and  
398 placed at three different corners within the home cage. The latency to retrieve each pup and the  
399 time spent licking the pups, crouching in the nest over the pups and performing nonmaternal  
400 behaviors such as self-grooming and digging were recorded over 15 min. Retrieval was defined  
401 as the animal picking up a pup and transporting it to the nest. Crouching was defined as the  
402 animal assuming the nursing posture. Nursing and licking were permitted whether they took  
403 place in the nest. All videos were analyzed using [BORIS software version 4.1.4](#).

404

405 **K-means clustering.** Clustering analysis of the behavioral data was performed using MATLAB  
406 Simulink 10b (The Mathworks, Inc., USA). Normality was verified and no outlier subjects were  
407 detected. To classify animals according to their maternal performance, a k-means clustering  
408 algorithm was used with crouching and digging times as behavioral markers. Digging was  
409 chosen because it is indicative of high maternal stress<sup>28,56</sup>. This algorithm iteratively grouped  
410 the animals by creating k initial centroids, assigning each animal to the closest centroid,  
411 iteratively re-calculating the centroids from the mean of its assigned animals and re-assigning  
412 the animals to each centroid until there were no more changes across iterations<sup>57</sup>. This clustering  
413 divided parous animals into a high maternal behavior group (with high crouching and low  
414 digging time) and low maternal behavior group (with low crouching and high digging time).

415

416 **Mouse brain template and atlas building.** For the MRI protocol, we developed a brain template  
417 and an atlas from the [AMBMC brain template](#) and the [Allen Mouse Brain Common Coordinate](#)  
418 [Framework](#), respectively (**Figure 1**). First, we down-sampled the AMBMC template and its  
419 associated atlases and the Allen Mouse Brain Atlas and its associated Nissl images to a suitable  
420 resolution for MRI analysis (60- $\mu$ m isotropic resolution) (**Figure 1**, step 1). Then, all images

421 were manually aligned to the anterior commissure/posterior commissure (AC/PC) axis, and the  
422 center of the images was defined relative to the AC (**Figure 1**, step 2). The resulting template  
423 was then segmented into GM, WM and CSF probability maps using the unified segmentation  
424 approach<sup>58</sup> of Statistical Parametric Mapping 8 ([SPM8](#)) and the mouse brain priors provided by  
425 the [SPMMouse toolbox](#) (**Figure 1**, step 3). In parallel, our T<sub>2</sub>-weighted anatomical images were  
426 realigned, coregistered, bias-corrected and normalized to our template. Using the SPMMouse  
427 toolbox, we also segmented the images as described above, and from these preprocessed  
428 images, we obtained a large set of 138 images for each tissue class (**Figure 1**, steps 4-7). From  
429 these images, we built population-specific GM, WM and CSF priors. To build these priors, for  
430 each tissue class, we applied a diffeomorphic anatomical registration using an exponentiated lie  
431 algebra (DARTEL) approach, which is an automated, unbiased, and nonlinear template-  
432 building algorithm<sup>59</sup> (**Figure 1**, step 8). This new set of population-specific tissue priors was  
433 used for both atlas building and final VBM preprocessing.

434 To normalize the Allen Mouse Brain Atlas to our brain template, we used the associated  
435 Nissl-stained images because (1) Nissl staining corresponds to the GM prior in terms of  
436 histology, and (2) this image was already coregistered to the atlas (**Figure 1**, step 4). Therefore,  
437 we applied the segmentation function provided by SPM8 using the GM prior previously  
438 calculated from the Nissl image to generate the “Nissl2template” normalization matrix. We  
439 used this matrix to normalize the atlas to the template, while avoiding interpolation to maintain  
440 the label indices as integers (**Figure 1**, step 7). Then, a visual inspection of each normalized  
441 label was carried out to assess whether the normalization process modified the position and  
442 volume of the structure too much. When necessary, holes were filled and labels were redrawn  
443 according to Paxinos and Franklin’s atlas and using the [FreeSurfer](#) package. Finally, the  
444 olfactory bulb and hind brain regions were completed, the corpus collosum and ventricles were  
445 drawn from the WM and CSF priors, and the cerebellum labels were replaced by the AMBMC

446 cerebellum labels, which are more accurate. Finally, the atlas image was symmetrized (left-  
447 right). Our mouse brain template, priors and atlas were normalized within the same space and  
448 with the same final resolution (60- $\mu$ m isotropic resolution), resulting in our final mouse brain  
449 atlas composed of a mosaic of 1320 ROIs covering the entire brain (**Supplemental Video 1**).

450

451 **VBM data preprocessing.** Previously preprocessed normalized T<sub>2</sub>-weighted data were  
452 segmented into GM, WM, and CSF within SPM8 using the images of the population-specific  
453 priors (**Figure 1**, step 9). Then, to produce a more accurate registration within each mouse as  
454 well as across all mice, a longitudinal VBM analysis was applied using the strategy described  
455 by Asami *et al*<sup>60</sup>. First, a *subject-specific* template was created by the DARTEL algorithm using  
456 the previous tissue class images (*i.e.*, GM, WM, and CSF maps) obtained from each mouse for  
457 the six time points. The DARTEL procedure releases *individual-specific* flow field maps,  
458 permitting the application of diffeomorphic normalization on images of each tissue class to  
459 spatially normalize each time point on a *subject-specific* template space. Each normalized tissue  
460 class image was modulated by the Jacobian determinant to account for the expansion and/or  
461 contraction of brain regions over time. Then, a *population-specific* template was created by the  
462 DARTEL algorithm using all *subject-specific* templates of the tissue class images. Here, the  
463 DARTEL procedure releases *population-specific* flow field maps, permitting the application of  
464 diffeomorphic normalization of each animal onto the images of each tissue class. Finally, tissue  
465 class images were modulated by the Jacobian determinant, and the final modulated GM images  
466 were spatially smoothed with an isotropic Gaussian kernel with a 3-mm full-width at half-  
467 maximum and convolved with GMC images to create GMC maps (**Figure 1**, steps 10-12).

468 **VBM statistics and analysis.** SPM8 was used to reveal the temporal and regional changes in  
469 the GMC maps. A second-level SPM analysis comprising a flexible factorial model, which is  
470 equivalent to a 2 $\times$ 2 mixed-model ANOVA with group as the between-subject factor and time

471 point as the within-subject factor, was used to compare the control *versus* the parous groups  
472 and the low *versus* high maternal behavior groups<sup>61</sup>. The factors included in the analysis were  
473 subjects, group (control *versus* parous, or low maternal behavior *versus* high maternal  
474 behavior), and time points (baseline, early gestation, late gestation, early lactation, late  
475 gestation, and weaning). A brain mask was used to constrain the analysis within the brain. For  
476 each cluster, the significance of the peak voxel was set as  $p < 0.01$  ( $t_{(126)} = 2.356$ , control *versus*  
477 parous;  $t_{(60)} = 2.39$ , low *versus* high maternal behavior), and the minimum cluster extent was  
478 set at 25 voxels. The results are presented on axial brain slice series generated by the [Xjview](#)  
479 SPM plugin. Corresponding surfacing results were produced with [BrainNet viewer 1.6](#)<sup>62</sup>,  
480 allowing the generation of both brain meshes and brain plots to visualize and videos.

481

482 ***Postprocessing statistical analysis.*** Cluster peaks revealed by the flexible factorial analyses  
483 were identified using our atlas and a *in situ* procedure developed with MATLAB Simulink 10b  
484 (The Mathworks, USA). For each comparison, clusters were binarized, and the obtained masks  
485 were used to extract GMC values of corresponding regions from the GMC map using the REX  
486 plugin. GMC data and behavioral measurements were then compiled and analyzed using  
487 GraphPad Prism 6.02 software. GMCs were compared between groups and for each time point  
488 using a two-way ANOVA with repeated measures followed by a two-stage setup method of  
489 Benjamini, Krieger and Yekutieli as recommended by the software. Maternal and nonmaternal  
490 behaviors of the low maternal and high maternal groups were compared using a  
491 multicomparison t-test with a false discovery rate (FDR) approach ( $Q = 1\%$ ). Correlation  
492 analyses were performed using a parametric two-tailed Pearson test. Specificity and selectivity  
493 analyses were performed using the ROC curve method. Statistical significance was defined as  
494  $p < 0.05$  (\*) for these analyses.

495 **Acknowledgments**

496 The authors acknowledge the regional council of Centre Val-de-Loire for funding this research  
497 through the IMACERVOREPRO grant (convention 201500104011, 2015-2018) awarded to  
498 Matthieu Keller.

499

500 **Author Contributions**

501 **D.A.B.** contributed to the atlas and template building, data analysis, drafted and revised the  
502 manuscript. **A.E.** contributed to the imaging sequence troubleshooting, data analysis and  
503 contributed to the critical revisions. **F.S.** contributed to the imaging sequence troubleshooting,  
504 data acquisitions and contributed to the analysis and critical revisions. **H.A., W.M., E.C.,**  
505 **M.M., S.M.** and **F.L.** contributed to the study conception and design and contributed to the  
506 critical revisions of the manuscript. **M.K.**, is the principal investigator of the study, raised the  
507 funding, coordinated the project and revised and validated the manuscript.

508 **References**

- 509 1. Numan, M. & Insel, T. R. *The neurobiology of parental behavior*. (Springer, 2003).
- 510 2. Lonstein, J. S., Lévy, F. & Fleming, A. S. Common and divergent psychobiological mechanisms underlying  
511 maternal behaviors in non-human and human mammals. *Horm. Behav.* **73**, 156–185 (2015).
- 512 3. Bridges, R. S. Neuroendocrine regulation of maternal behavior. *Front. Neuroendocrinol.* **36**, 178–196 (2015).
- 513 4. Kohl, J. & Dulac, C. Neural control of parental behaviors. *Curr. Opin. Neurobiol.* **49**, 116–122 (2018).
- 514 5. Kohl, J., Autry, A. E. & Dulac, C. The neurobiology of parenting: A neural circuit perspective. *BioEssays* **39**,  
515 e201600159 (2017).
- 516 6. Lévy, F. & Keller, M. Olfactory mediation of maternal behavior in selected mammalian species. *Behav. Brain*  
517 *Res.* **200**, 336–345 (2009).
- 518 7. Numan, M. & Stolzenberg, D. S. Medial preoptic area interactions with dopamine neural systems in the control  
519 of the onset and maintenance of maternal behavior in rats. *Front. Neuroendocrinol.* **30**, 46–64 (2009).
- 520 8. Afonso, V. M., Sison, M., Lovic, V. & Fleming, A. S. Medial prefrontal cortex lesions in the female rat affect  
521 sexual and maternal behavior and their sequential organization. *Behav. Neurosci.* **121**, 515–526 (2007).
- 522 9. Febo, M. A bold view of the lactating brain: functional magnetic resonance imaging studies of suckling in  
523 awake dams. *J. Neuroendocrinol.* **23**, 1009–1019 (2011).
- 524 10. Pereira, M. & Morrell, J. I. Functional Mapping of the Neural Circuitry of Rat Maternal Motivation: Effects of  
525 Site-Specific Transient Neural Inactivation: Mapping maternal motivation circuitry. *J. Neuroendocrinol.* **23**,  
526 1020–1035 (2011).
- 527 11. Brunton, P. J. & Russell, J. A. The expectant brain: adapting for motherhood. *Nat. Rev. Neurosci.* **9**, 11–25  
528 (2008).
- 529 12. Kinsley, C. H. & Lambert, K. G. Reproduction-Induced Neuroplasticity: Natural Behavioural and Neuronal  
530 Alterations Associated with the Production and Care of Offspring. *J. Neuroendocrinol.* **20**, 515–525 (2008).
- 531 13. Lévy, F., Gheusi, G. & Keller, M. Plasticity of the Parental Brain: A Case for Neurogenesis: Parental behaviour  
532 and neurogenesis. *J. Neuroendocrinol.* **23**, 984–993 (2011).
- 533 14. Akbari, E. M., Chatterjee, D., Lévy, F. & Fleming, A. S. Experience-dependent cell survival in the maternal  
534 rat brain. *Behav. Neurosci.* **121**, 1001–1011 (2007).
- 535 15. Hoekzema, E. *et al.* Pregnancy leads to long-lasting changes in human brain structure. *Nat. Neurosci.* **20**, 287  
536 (2017).
- 537 16. Kohl, J. *et al.* Functional circuit architecture underlying parental behaviour. *Nature* **556**, 326–331 (2018).
- 538 17. Ashburner, J. & Friston, K. J. Unified segmentation. *NeuroImage* **26**, 839–851 (2005).
- 539 18. Sawiak, S. J., Wood, N. I., Williams, G. B., Morton, A. J. & Carpenter, T. A. Voxel-based morphometry with  
540 templates and validation in a mouse model of Huntington’s disease. *Magn. Reson. Imaging* **31**, 1522–1531 (2013).
- 541 19. Sawiak, S. J., Picq, J.-L. & Dhenain, M. Voxel-based morphometry analyses of in vivo MRI in the aging mouse  
542 lemur primate. *Front. Aging Neurosci.* **6**, (2014).
- 543 20. Keifer Jr, O. P. *et al.* Voxel-based morphometry predicts shifts in dendritic spine density and morphology with  
544 auditory fear conditioning. *Nat. Commun.* **6**, (2015).
- 545 21. Lein, E. S. *et al.* Genome-wide atlas of gene expression in the adult mouse brain. *Nature* **445**, 168–176 (2007).
- 546 22. Ullmann, J. F. P. *et al.* Segmentation of the C57BL/6J mouse cerebellum in magnetic resonance images.  
547 *NeuroImage* **62**, 1408–1414 (2012).
- 548 23. Richards, K. *et al.* Segmentation of the mouse hippocampal formation in magnetic resonance images.  
549 *NeuroImage* **58**, 732–740 (2011).
- 550 24. Watson, C. *et al.* An ontologically consistent MRI-based atlas of the mouse diencephalon. *NeuroImage* **157**,  
551 275–287 (2017).
- 552 25. Ullmann, J. F. P., Watson, C., Janke, A. L., Kurniawan, N. D. & Reutens, D. C. A segmentation protocol and  
553 MRI atlas of the C57BL/6J mouse neocortex. *NeuroImage* **78**, 196–203 (2013).
- 554 26. Wang, Q. *et al.* The Allen Mouse Brain Common Coordinate Framework: A 3D Reference Atlas. *Cell* **181**,  
555 936-953.e20 (2020).
- 556 27. Paxinos and Franklin’s the Mouse Brain in Stereotaxic Coordinates, Compact - 5th Edition.  
557 [https://www.elsevier.com/books/paxinos-and-franklins-the-mouse-brain-in-stereotaxic-coordinates-](https://www.elsevier.com/books/paxinos-and-franklins-the-mouse-brain-in-stereotaxic-coordinates-compact/franklin/978-0-12-816159-3)  
558 [compact/franklin/978-0-12-816159-3](https://www.elsevier.com/books/paxinos-and-franklins-the-mouse-brain-in-stereotaxic-coordinates-compact/franklin/978-0-12-816159-3).
- 559 28. Deacon, R. M. J. Digging and marble burying in mice: simple methods for *in vivo* identification of biological  
560 impacts. *Nat. Protoc.* **1**, 122 (2006).

- 561 29. Tsuneoka, Y. *et al.* Neurotransmitters and neuropeptides in gonadal steroid receptor-expressing cells in medial  
562 preoptic area subregions of the male mouse. *Sci. Rep.* **7**, 1–16 (2017).
- 563 30. McHenry, J. A., Rubinow, D. R. & Stuber, G. D. Maternally responsive neurons in the bed nucleus of the *stria*  
564 *terminalis* and medial preoptic area: Putative circuits for regulating anxiety and reward. *Front. Neuroendocrinol.*  
565 **38**, 65–72 (2015).
- 566 31. Olazábal, D. E. *et al.* Flexibility and adaptation of the neural substrate that supports maternal behavior in  
567 mammals. *Neurosci. Biobehav. Rev.* **37**, 1875–1892 (2013).
- 568 32. Bridges, R. S. & Hays, L. E. Steroid-induced alterations in mRNA expression of the long form of the prolactin  
569 receptor in the medial preoptic area of female rats: Effects of exposure to a pregnancy-like regimen of progesterone  
570 and estradiol. *Brain Res. Mol. Brain Res.* **140**, 10–16 (2005).
- 571 33. Lonstein, J. S. & De Vries, G. J. Maternal behaviour in lactating rats stimulates c-fos in glutamate  
572 decarboxylase-synthesizing neurons of the medial preoptic area, ventral bed nucleus of the *stria terminalis*, and  
573 ventrocaudal periaqueductal gray. *Neuroscience* **100**, 557–568 (2000).
- 574 34. Miceli, M. O., Fleming, A. S. & Malsbury, C. W. Disruption of maternal behaviour in virgin and postparturient  
575 rats following sagittal plane knife cuts in the preoptic area-hypothalamus. *Behav. Brain Res.* **9**, 337–360 (1983).
- 576 35. Lee, A., Clancy, S. & Fleming, A. S. Mother rats bar-press for pups: effects of lesions of the mpoa and limbic  
577 sites on maternal behavior and operant responding for pup-reinforcement. *Behav. Brain Res.* **100**, 15–31 (1999).
- 578 36. El Majdoubi, M., Poulain, D. A. & Theodosis, D. T. Activity-dependent morphological synaptic plasticity in  
579 an adult neurosecretory system: magnocellular oxytocin neurons of the hypothalamus. *Biochem. Cell Biol.*  
580 *Biochim. Biol. Cell.* **78**, 317–327 (2000).
- 581 37. D’Cunha, T. M., King, S. J., Fleming, A. S. & Lévy, F. Oxytocin receptors in the nucleus accumbens shell are  
582 involved in the consolidation of maternal memory in postpartum rats. *Horm. Behav.* **59**, 14–21 (2011).
- 583 38. Insel, T. R. & Harbaugh, C. R. Lesions of the hypothalamic paraventricular nucleus disrupt the initiation of  
584 maternal behavior. *Physiol. Behav.* **45**, 1033–1041 (1989).
- 585 39. Numan, M. & Corodimas, K. P. The effects of paraventricular hypothalamic lesions on maternal behavior in  
586 rats. *Physiol. Behav.* **35**, 417–425 (1985).
- 587 40. Olazábal, D. E., Kalinichev, M., Morrell, J. I. & Rosenblatt, J. S. MPOA cytotoxic lesions and maternal  
588 behavior in the rat: effects of midpubertal lesions on maternal behavior and the role of ovarian hormones in  
589 maturation of MPOA control of maternal behavior. *Horm. Behav.* **41**, 126–138 (2002).
- 590 41. Freeman, M. E., Kanyicska, B., Lerant, A. & Nagy, G. Prolactin: structure, function, and regulation of  
591 secretion. *Physiol. Rev.* **80**, 1523–1631 (2000).
- 592 42. Cservenák, M. *et al.* Thalamic neuropeptide mediating the effects of nursing on lactation and maternal  
593 motivation. *Psychoneuroendocrinology* **38**, 3070–3084 (2013).
- 594 43. Kinsley, C. H. *et al.* Motherhood and the hormones of pregnancy modify concentrations of hippocampal  
595 neuronal dendritic spines. *Horm. Behav.* **49**, 131–142 (2006).
- 596 44. Pawluski, J. L. & Galea, L. A. M. Hippocampal morphology is differentially affected by reproductive  
597 experience in the mother. *J. Neurobiol.* **66**, 71–81 (2006).
- 598 45. Pawluski, J. L., Walker, S. K. & Galea, L. A. M. Reproductive experience differentially affects spatial reference  
599 and working memory performance in the mother. *Horm. Behav.* **49**, 143–149 (2006).
- 600 46. Gogolla, N. The insular cortex. *Curr. Biol.* **27**, R580–R586 (2017).
- 601 47. Mak, G. K. & Weiss, S. Paternal recognition of adult offspring mediated by newly generated CNS neurons.  
602 *Nat. Neurosci.* **13**, 753–758 (2010).
- 603 48. Larsen, C. M. & Grattan, D. R. Prolactin-induced mitogenesis in the subventricular zone of the maternal brain  
604 during early pregnancy is essential for normal postpartum behavioral responses in the mother. *Endocrinology* **151**,  
605 3805–3814 (2010).
- 606 49. Sakamoto, M. *et al.* Continuous neurogenesis in the adult forebrain is required for innate olfactory responses.  
607 *Proc. Natl. Acad. Sci. U. S. A.* **108**, 8479–8484 (2011).
- 608 50. Kelly, J. R. *et al.* Breaking down the barriers: the gut microbiome, intestinal permeability and stress-related  
609 psychiatric disorders. *Front. Cell. Neurosci.* **9**, 392 (2015).
- 610 51. Arentsen, T. *et al.* The bacterial peptidoglycan-sensing molecule Pglyrp2 modulates brain development and  
611 behavior. *Mol. Psychiatry* **22**, 257–266 (2017).
- 612 52. Barrière, D. A. *et al.* Structural and functional alterations in the retrosplenial cortex following neuropathic pain.  
613 *Pain* (2019) doi:10.1097/j.pain.0000000000001610.

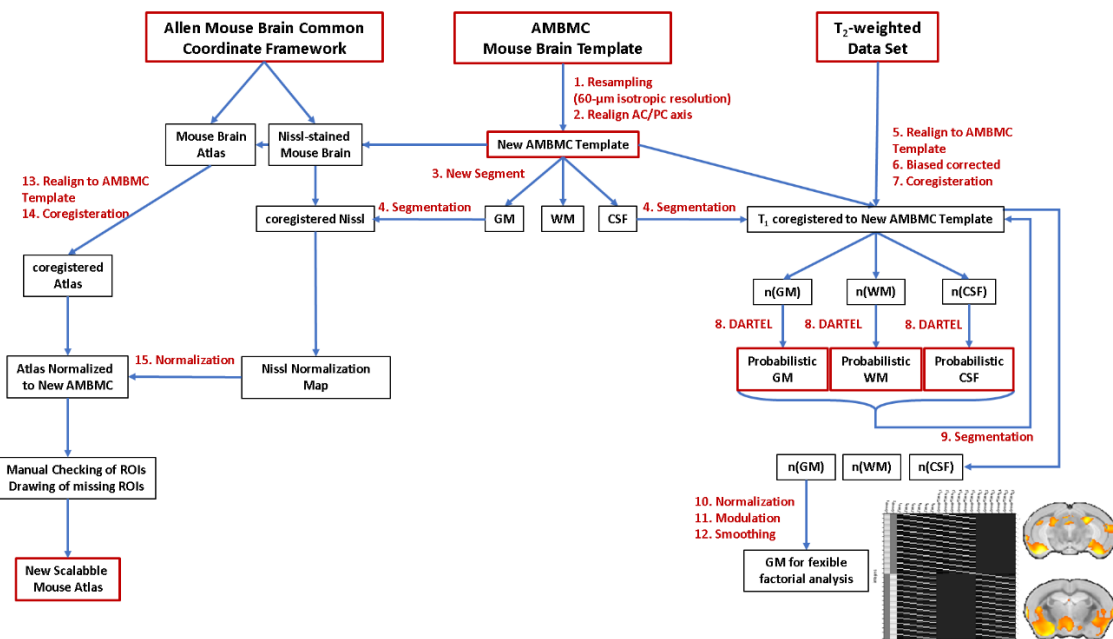
- 614 53. DiIorio, G., Brown, J. J., Borrello, J. A., Perman, W. H. & Shu, H. H. Large angle spin-echo imaging. *Magn.*  
615 *Reson. Imaging* **13**, 39–44 (1995).
- 616 54. Ma, Y. *et al.* In vivo 3D digital atlas database of the adult C57BL/6J mouse brain by magnetic resonance  
617 microscopy. *Front. Neuroanat.* **2**, (2008).
- 618 55. Keller, M., Pawluski, J. L., Brock, O., Douhard, Q. & Bakker, J. The  $\alpha$ -fetoprotein knock-out mouse model  
619 suggests that parental behavior is sexually differentiated under the influence of prenatal estradiol. *Horm. Behav.*  
620 **57**, 434–440 (2010).
- 621 56. van den Brom, C. E. *et al.* Altered myocardial substrate metabolism is associated with myocardial dysfunction  
622 in early diabetic cardiomyopathy in rats: studies using positron emission tomography. *Cardiovasc. Diabetol.* **8**, 39  
623 (2009).
- 624 57. Magalhães, R. *et al.* The dynamics of stress: a longitudinal MRI study of rat brain structure and connectome.  
625 *Mol. Psychiatry* (2017) doi:10.1038/mp.2017.244.
- 626 58. Ashburner, J. & Friston, K. J. Voxel-based morphometry--the methods. *NeuroImage* **11**, 805–821 (2000).
- 627 59. Ashburner, J. A fast diffeomorphic image registration algorithm. *NeuroImage* **38**, 95–113 (2007).
- 628 60. Asami, T. *et al.* Longitudinal loss of gray matter volume in patients with first-episode schizophrenia: DARTEL  
629 automated analysis and ROI validation. *NeuroImage* **59**, 986–996 (2012).
- 630 61. Barrière, D. A. *et al.* In vivo magnetic resonance imaging reveals the effect of gonadal hormones on  
631 morphological and functional brain sexual dimorphisms in adult sheep. *Psychoneuroendocrinology* **109**, 104387  
632 (2019).
- 633 62. Xia, M., Wang, J. & He, Y. BrainNet Viewer: a network visualization tool for human brain connectomics. *PLoS*  
634 *One* **8**, e68910 (2013).

635 **Tables**

<i>Ex vivo / In vivo</i>	Strain	Sex	Age (days)	Number of animals	Magnetic field intensity	Anatomical contrast	Spatial resolution	MRI Template	Atlas	Regions of interest	Tissue Probability maps	References
<i>Ex vivo</i>	C57BL/6J	Male	63	6	9.4 Tesla	T <sub>2</sub> PD DW	90 x 90 x 90 μm <sup>3</sup>	Yes	Yes	21	No	<i>Ali et al, 2005</i>
<i>In vivo</i>	C57BL/6J	Male	100	6	11.7 Tesla	T <sub>2</sub>	60 x 60 x 60 μm <sup>3</sup>	Yes	Yes	NA	No	<i>MacKenzie-Graham et al, 2004</i>
<i>Ex vivo</i>	129S1/SvImJ	Male	56	9	7 Tesla	T <sub>2</sub>	60 x 60 x 60 μm <sup>3</sup>	Yes	Yes	9	No	<i>Kovačević et al, 2005</i>
<i>Ex vivo</i>	C57BL/6J	NA	P0	8	11.7 Tesla	T <sub>2</sub>	40 x 40 x 40 μm <sup>3</sup>	Yes	Yes	12	Yes	<i>Lee et al, 2005</i>
<i>In vivo</i>	C57BL/6J	Male	84-98	12	9.4 Tesla	T <sub>2</sub>	100 x 100 x 100 μm <sup>3</sup>	Yes	Yes	20	No	<i>Ma et al, 2008</i>
<i>In vivo</i>	C3H/HeSnJ	NA	77	15	7 Tesla	T <sub>1</sub>	156 x 156 x 156 μm <sup>3</sup>	Yes	Yes	6	No	<i>Boek et al, 2006</i>
<i>Ex vivo</i>	129S1/SvImJ C57Bl6 CD1	Male	126	27	7 Tesla	T <sub>2</sub>	60 x 60 x 60 μm <sup>3</sup>	Yes	Yes	42	No	<i>Chen et al, 2008</i>
<i>Ex vivo</i>	C57BL/6J	NA	63	6	9.4 Tesla	T <sub>1</sub> T <sub>2</sub>	21.5 x 21.5 x 21.5 μm <sup>3</sup> 43 x 43 x 43 μm <sup>3</sup>	Yes	Yes	33	No	<i>Badea et al, 2008</i>
<i>Ex vivo</i>	C57BL/6J	20 males 20 females	84	40	7 Tesla	T <sub>2</sub>	32 x 32 x 32 μm <sup>3</sup>	Yes	Yes	62	No	<i>Dorr et al, 2008</i>
<i>Ex vivo</i>	C57BL/6J and BXD	Male	63	12	9.4 Tesla	T <sub>1</sub> T <sub>2</sub>	21.5 x 21.5 x 21.5 μm <sup>3</sup> 43 x 43 x 43 μm <sup>3</sup>	Yes	Yes	20	No	<i>Sharief et al, 2008</i>
<i>Ex vivo</i>	C57BL/6J	Male	66-78	14	9.4 Tesla	T <sub>1</sub> T <sub>2</sub> T <sub>2</sub> *	21.5 x 21.5 x 21.5 μm <sup>3</sup>	Yes	Yes	37	No	<i>Johnson et al, 2010</i>
<i>Ex vivo</i>	C57BL/6J	Male	84	18	16.4 Tesla	T1/T2*	30 x 30 x 30 μm <sup>3</sup>	Yes	Yes (Partial: hippocampus)	40	No	<i>Richards et al, 2011</i>
<i>Ex vivo</i>	C57BL/6J	Male	84	18	16.4 Tesla	T1/T2*	30 x 30 x 30 μm <sup>3</sup>	Yes	Yes (Partial: cerebellum)	38	No	<i>Ullman et al, 2013</i>
<i>Ex vivo</i>	C57BL/6J	Male	84	18	16.4 Tesla	T1/T2*	30 x 30 x 30 μm <sup>3</sup>	Yes	Yes (Partial: basal ganglia)	35	No	<i>Ullman et al, 2013</i>
<i>Ex vivo</i>	C57BL/6J	Male	84	18	16.4 Tesla	T1/T2*	30 x 30 x 30 μm <sup>3</sup>	Yes	Yes (Partial: neocortex)	74	No	<i>Ullman et al, 2013</i>
<i>In vivo</i>	C57BL/6J	Male	126	82	4.7 Tesla	T <sub>2</sub>	70 x 70 x 70 μm <sup>3</sup>	No	NA	NA	Yes	<i>Sawiak et al, 2013</i>
<i>Ex vivo</i>	C57BL/6J	Male	84	18	16.4 Tesla	T1/T2*	30 x 30 x 30 μm <sup>3</sup>	Yes	Yes (Partial: diencephalon)	89	No	<i>Watson et al, 2017</i>
<i>Ex vivo</i>	C57BL/6J	1.051 males 621 female	77	1675	NA	NA	10 x 10 x 10 μm <sup>3</sup>	No	Yes	1327	No	<i>Wang et al, 2020</i>

636

637 **Table 1.** Comparison of mouse brain resources currently available in the literature (NA = not  
638 available).

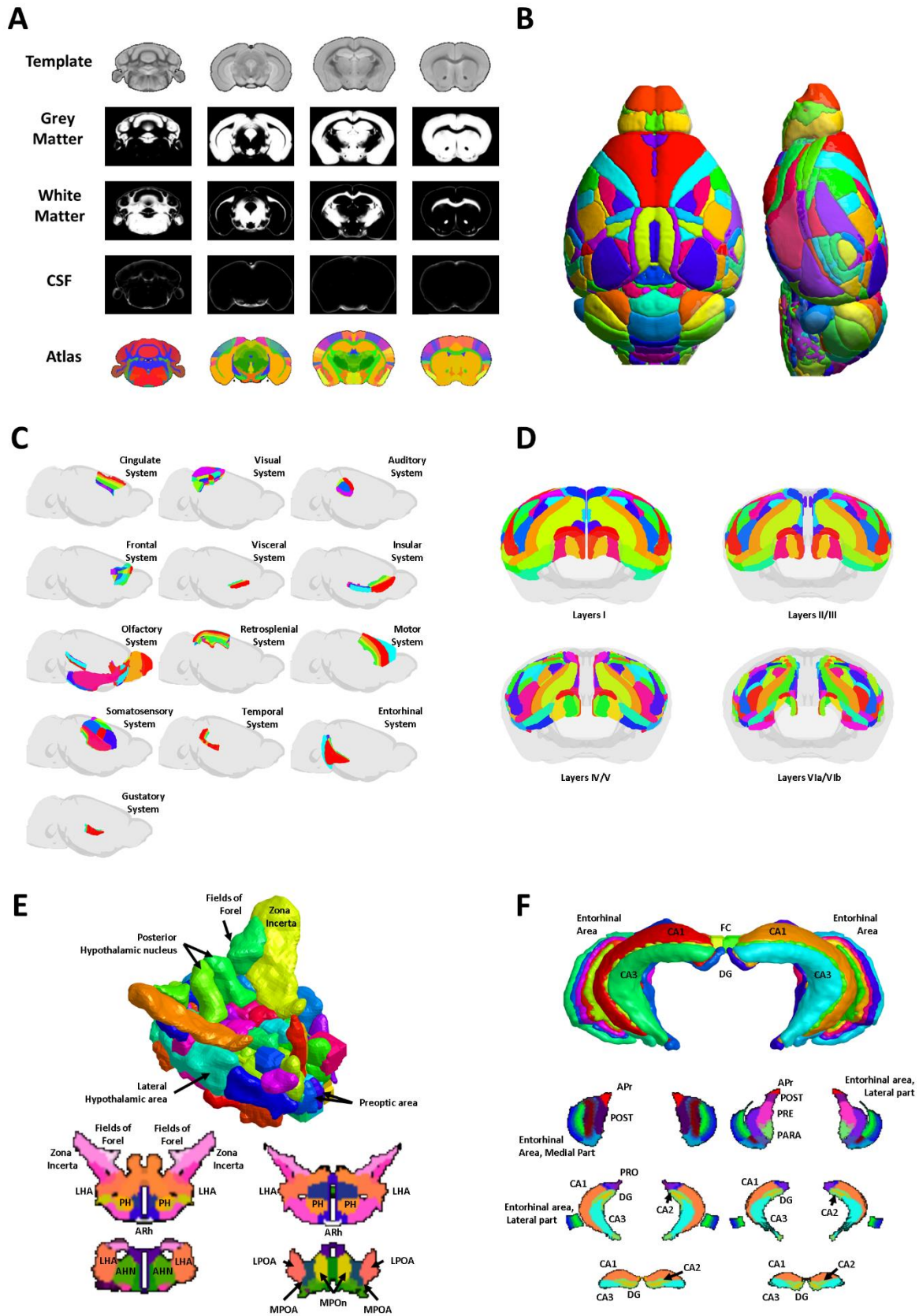


640

641 **Figure 1.** Processing of mouse brain templates and building an atlas from the AMBMC  
 642 template and Allen Brain Atlas for data analysis and visualization. To create our resources, we  
 643 used both AMBMC mouse brain template and the mouse Allen Brain Atlas and its associated  
 644 Nissl images. (1) We down-sampled to a suitable resolution for MRI analysis (60- $\mu\text{m}$  isotropic  
 645 resolution) and (2) realign in the AC/PC axis. The resulting template was then segmented into  
 646 GM, WM and CSF probability maps (3). These probability maps were used to segment all the  
 647 images which have been previously normalized to the template (5,6,7). We obtained a large set  
 648 of 138 images for each tissue class which have been used to build a population-specific GM,  
 649 WM and CSF priors. using an exponentiated lie algebra (DARTEL) approach (8). This new set  
 650 of population-specific tissue priors was used to segment again normalized T<sub>2</sub> images (9) for the  
 651 final VBM preprocessing (10, 11, 12). To normalize the Allen Brain Atlas, we manually realign  
 652 (13) and normalized the associated Nissl-stain mouse brain using the GM priors generated  
 653 previously (14, 15). Both linear and nonlinear transformations have been applied to the Allen  
 654 mouse brain atlas. Then, a visual inspection of each normalized label was carried out and, when  
 655 necessary, redrawn according to Paxinos and Franklin's atlas. Finally, the olfactory bulb and

656 hind brain regions were completed, the *corpus callosum* and ventricles were drawn from the  
657 WM and CSF priors, and the cerebellum labels were replaced by the AMBMC cerebellum  
658 labels.

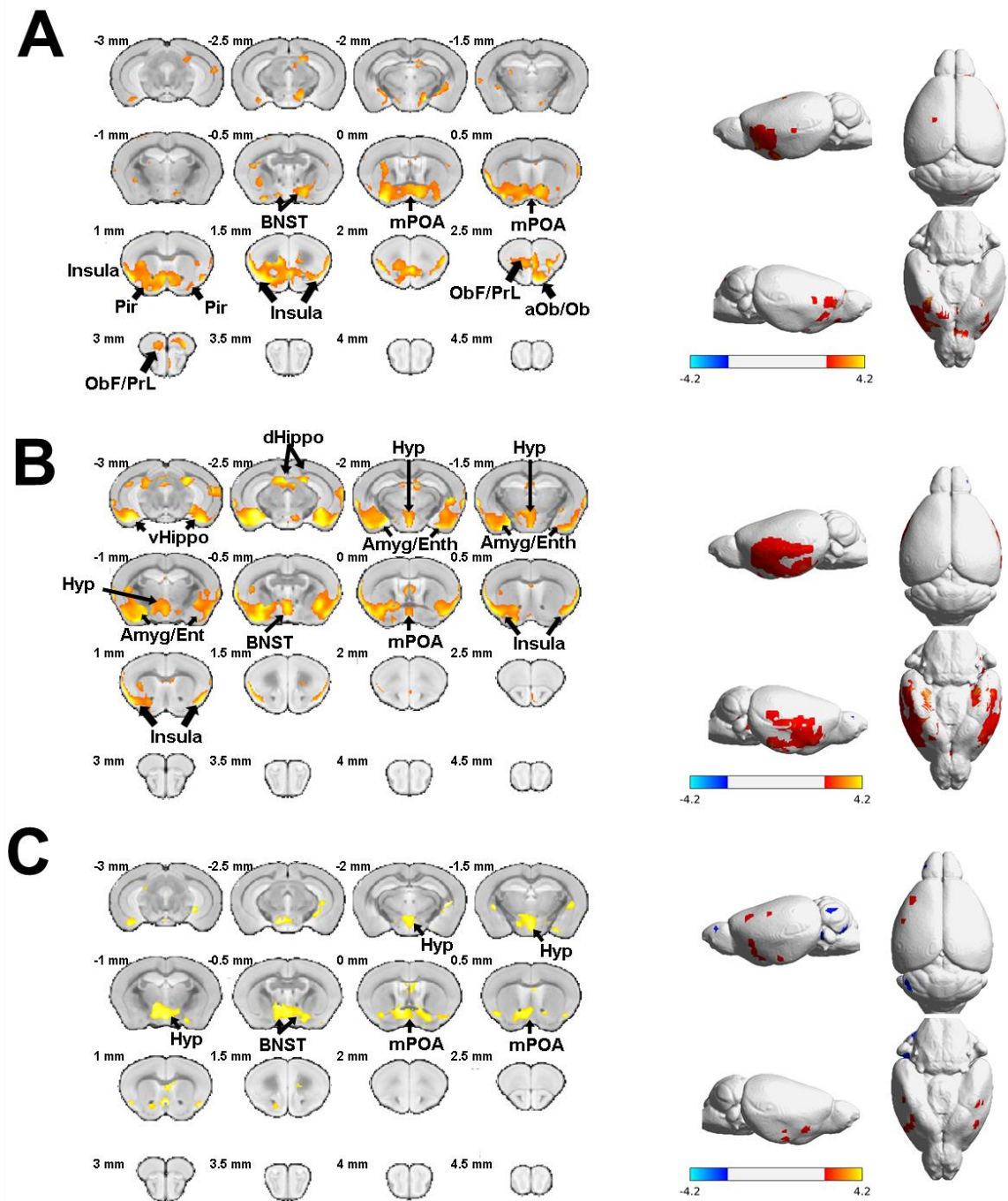
659 AMBMC = Australian Mouse Brain Mapping Consortium mouse brain template, AC/PC =  
660 anterior commissure/posterior commissure, CSF = cerebrospinal fluid, GM = gray matter, WM  
661 = white matter.



662

663 **Figure 2.** Details of the mouse brain template and atlas. (A) Coronal slices of the anatomical  
 664 template of the mouse brain and the corresponding gray matter, white matter and cerebrospinal

665 fluid probabilistic maps and the associated anatomical atlas (60- $\mu$ m isotropic resolution). **(B)**  
666 Dorsal (left panel) and lateral (right panel) 3D representations of the anatomical mouse brain  
667 atlas. **(C)** Lateral views of the cortical areas after normalization of the Allen Mouse Brain Atlas  
668 to the AMBMC anatomical template. The cortex was segmented into cortical areas such as the  
669 cingulate, visual, auditory, frontal, visceral, insular, olfactory, retrosplenial, motor,  
670 somatosensory, temporal, entorhinal and gustatory systems. Each area was subdivided into  
671 secondary areas (*e.g.*, primary and secondary motor cortices) or structural areas (*i.e.*, agranular,  
672 dysgranular, agranular/dysgranular, granular and posterior agranular insular cortices). **(D)** The  
673 four images depict the different cortical layers (I, II/III, IV/V and VIa/VIb). **(E and F)** 3D  
674 rendering and axial sections of subcortical structures (hypothalamus and hippocampus).  
675 Legend for labeled regions: Hypothalamus: *ARh* = *arcuate hypothalamic nucleus*; *LHA* =  
676 *lateral hypothalamic area*; *LPOA* = *lateral preoptic area*; *MPOA* = *medial preoptic area*;  
677 *MPOn* = *medial preoptic nucleus*; *PH* = *posterior hypothalamic nucleus*. *AHN* = *anterior*  
678 *hypothalamic nucleus*.  
679 Hippocampus: *Apr* = *area prostriata*; *CA1*, *CA2*, *CA3* = *cornu ammonis areas 1, 2 and 3*; *DG*  
680 = *dentate gyrus*; *FC* = *fasciola cinerea*; *PARA* = *parasubiculum*; *POST* = *postsubiculum*; *PRO*  
681 = *prosubiculum*; *PRE* = *presubiculum*. For further details, see  
682 [https://www.nitrc.org/projects/tmbta\\_2019](https://www.nitrc.org/projects/tmbta_2019).

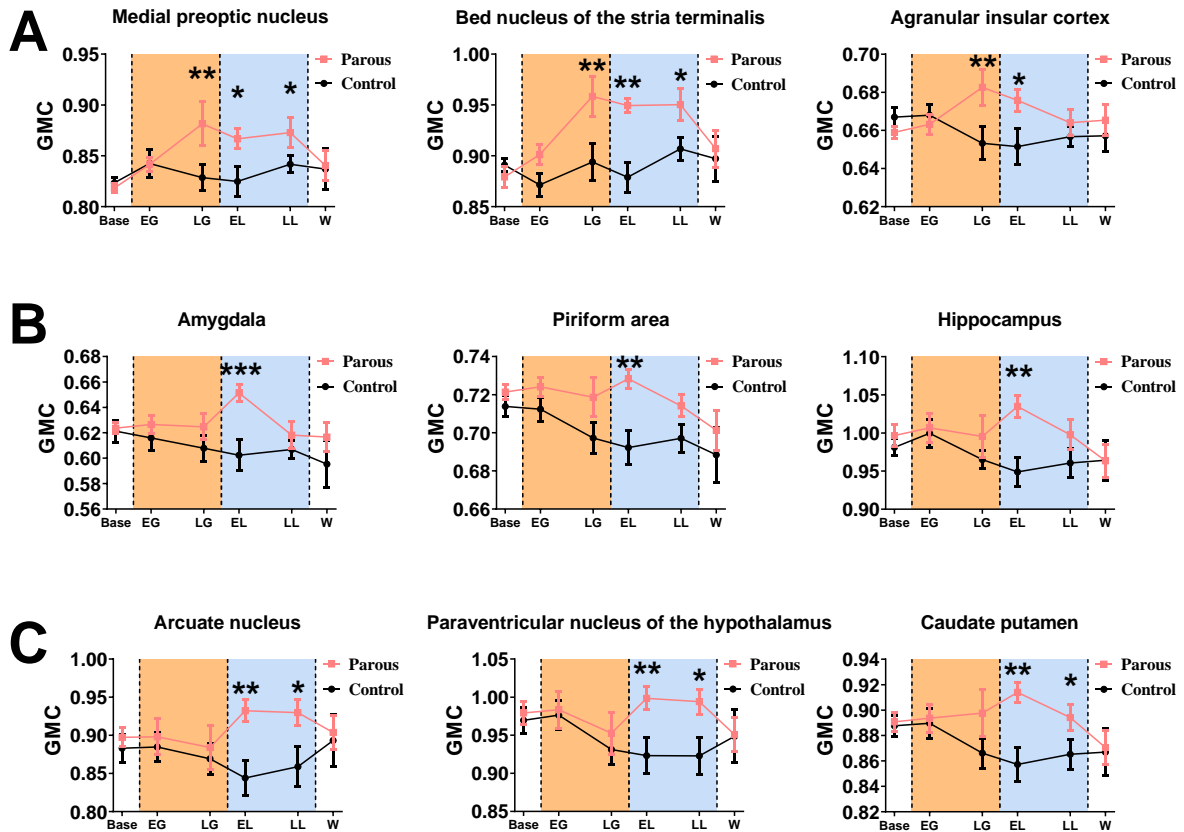


683

684 **Figure 3.** Longitudinal effects of the reproductive cycle on brain morphometry. Coronal slices  
 685 (at left) and brain plots (at right) showing gray matter concentration (GMC) differences between  
 686 control and parous animals at the end of gestation (A) and during early lactation (B) and late  
 687 lactation (C).

688 SPM flexible factorial analysis revealed an interaction between control mice and parous mice  
 689 in the late gestation period (A), early lactation period (B) and late lactation period (C); voxel-

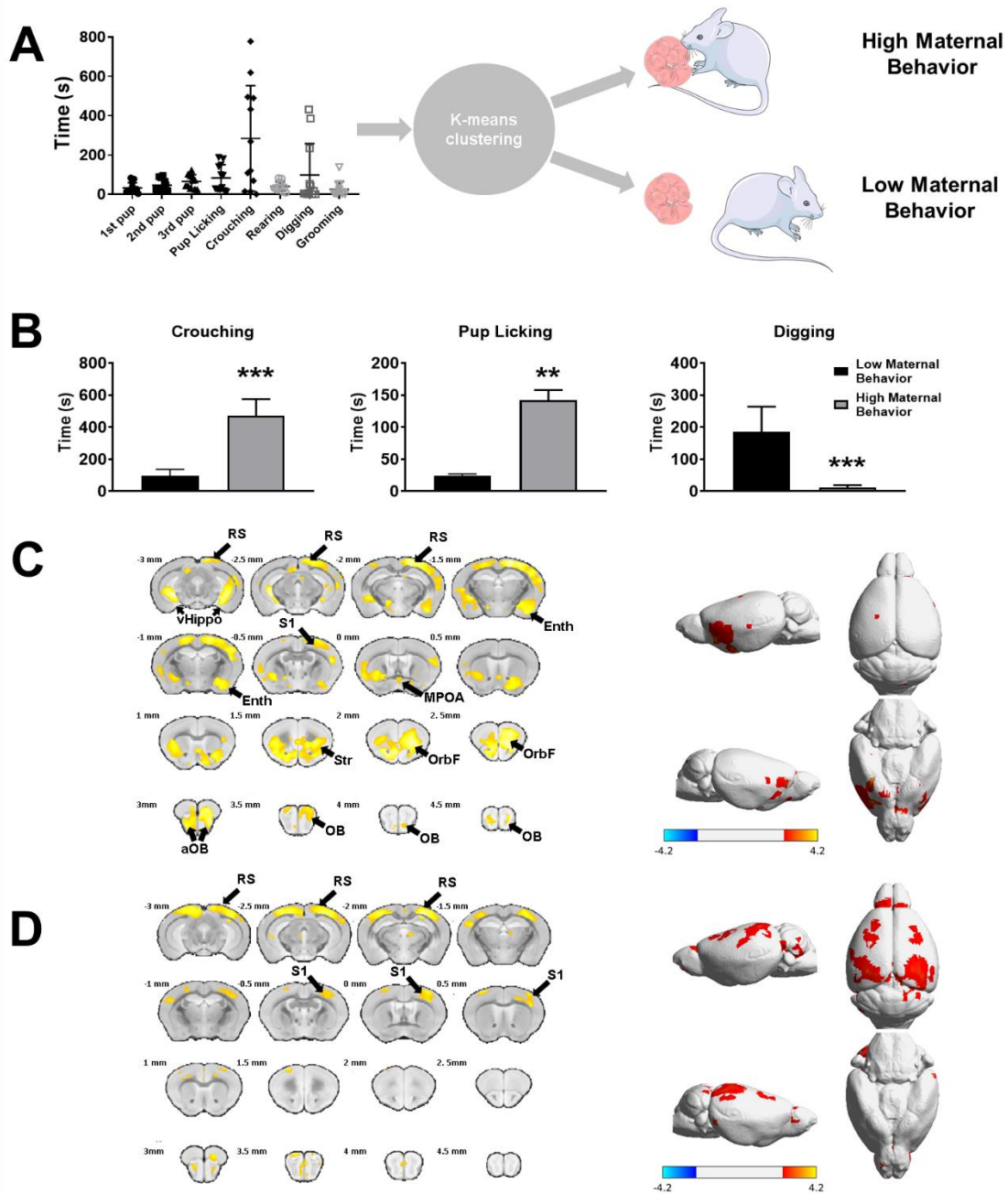
690 level threshold  $p < 0.01$ ,  $t_{(126)} = 2.356$ , cluster threshold = 25 voxels. *BNST* = *bed nucleus of*  
691 *the stria terminalis*; *Hyp* = *hypothalamus*; *mPOA* = *medial preoptic area*; *dHippo* = *dorsal*  
692 *hippocampus*; *ObF/PrL* = *orbitofrontal/prelimbic area*; *aOb/Ob* = *accessory olfactory*  
693 *nucleus/olfactory bulb*; *Pir* = *piriform cortex*; *Amyg/Ent* = *amygdala/entorhinal cortex*.



694

695 **Figure 4.** Longitudinal time course analysis of gray matter concentration (GMC) over the  
 696 reproductive cycle. Time course comparisons in GMC between the control (black dots and  
 697 lines) and parous (red dots and lines) groups showing 3 different time profiles. (A) GMC values  
 698 within the medial preoptic area, the bed nucleus of *stria terminalis* (BNST) and the agranular  
 699 insular cortex reveal a significant increase in GMC during the late gestation (LG) period  
 700 maintained until weaning (W). (B) Specific and transient increases in GMCs are observed in  
 701 the amygdala, the piriform area and the hippocampus during early lactation (EL). (C) The  
 702 arcuate nucleus, PVN and caudate putamen display an increase in GMC through both EL and  
 703 late lactation (LL) periods.

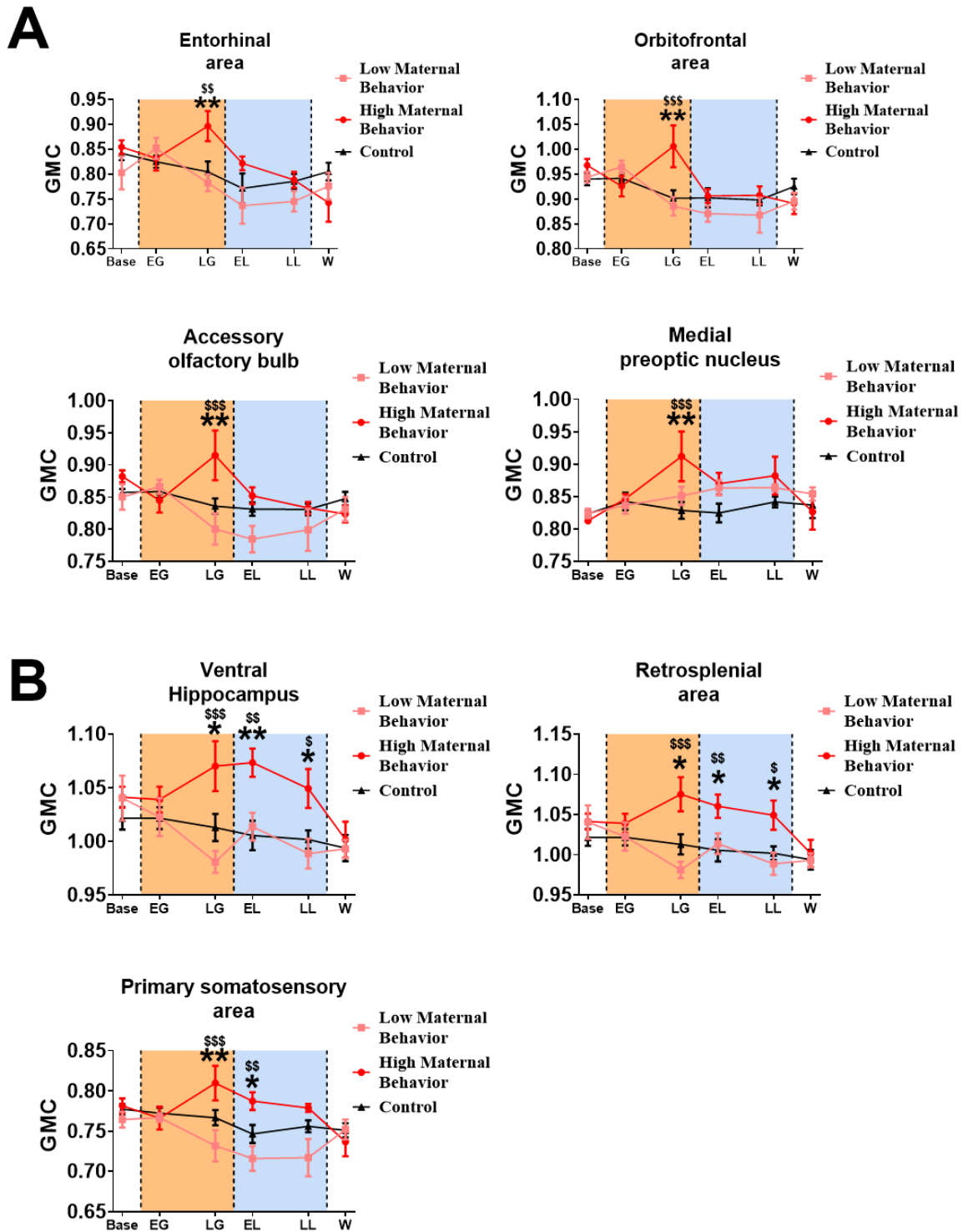
704 Orange and blue areas represent the gestation and lactation periods, respectively. Data are  
 705 expressed as the mean  $\pm$  standard error of the mean (SEM); two-way ANOVA followed by  
 706 Holm-Sidak multiple comparisons test; \* $p < 0.05$ , \*\*  $p < 0.01$  and \*\*\*  $p < 0.001$ , compared  
 707 with control mice.



708

709 **Figure 5.** Distribution of animals according to the quality of their maternal behavior assessed  
 710 with the pup retrieval test and brain morphometric. K-means clustering of parous animals to  
 711 classify mice into low and high maternal behavior groups based on behavior during the pup  
 712 retrieval test (A). Comparisons between the low and high maternal behavior groups revealed  
 713 significant differences in crouching, pup-licking and digging times (B). Brain slices (left panel)  
 714 and brain plots (right panel) comparing gray matter concentration (GMC) modifications and

715 surface maps of GMC differences between females exhibiting low and those exhibiting high  
716 maternal behavior at the end of the gestation period (C) and early lactation period (D).  
717 Low and high maternal behavioral data were compared using a Student's t-test with post hoc  
718 corrections for multiple comparisons using an FDR approach ( $Q = 1\%$ ) and are expressed as  
719 the mean  $\pm$  SEM; \*\*  $p < 0.01$  and \*\*\*  $p < 0.001$ . SPM flexible factorial analysis revealed an  
720 interaction between low and high maternal behavior parous mice in the late gestation period  
721 (A) and early lactation period (B); voxel-level threshold  $p < 0.01$ ,  $t_{(60)} = 2.39$ , cluster threshold  
722 = 25 voxels. *RS* = retrosplenial cortex; *vHippo* = ventral hippocampus; *S1* = primary  
723 somatosensory cortex; *aOB* = accessory olfactory bulb; *OB* = olfactory bulb; *Pir* = piriform  
724 cortex; *EntH* = entorhinal cortex; *Str* = striatum; *OrbF* = orbitofrontal cortex.

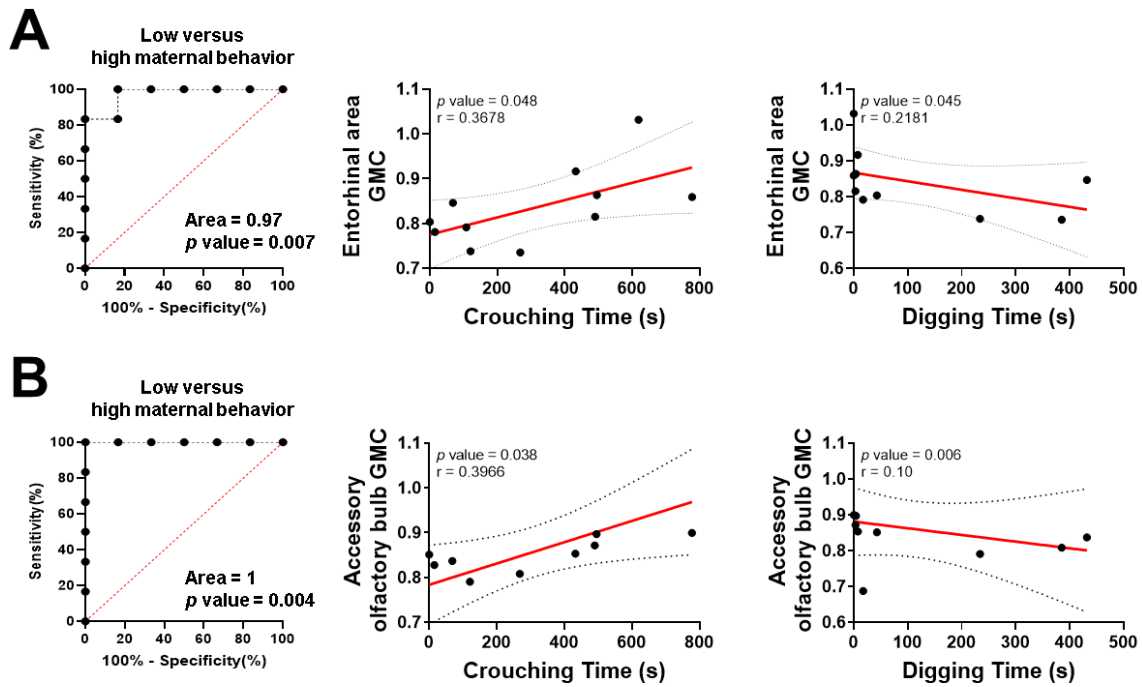


725

726 **Figure 6.** Longitudinal analysis in gray matter concentration (GMC) during the reproductive  
 727 cycle in control females and females exhibiting low or high maternal behavior. Time-course  
 728 comparison of GMC between the control (black dots and lines), low maternal behavior (pink  
 729 dots and lines) and high maternal behavior (red dots and lines) groups revealed two types of

730 time profile. GMC analysis in the entorhinal area, orbitofrontal area, the accessory olfactory  
731 bulb and the medial preoptic nucleus revealed an acute and specific increase in GMC values in  
732 the high maternal behavior group at the late gestation period (**A**). In contrast, GMC analysis in  
733 the ventral hippocampus, the retrosplenial area and the primary somatosensory area revealed  
734 an increase in GMC in the high maternal behavior group at the late gestation period, and this  
735 increase was maintained until weaning (**B**).

736 Orange and blue areas represent the gestation and lactation periods, respectively. Data were  
737 compared using a two-way ANOVA followed by Holm-Sidak multiple comparisons test and  
738 expressed as the mean  $\pm$  SEM; \*  $p < 0.05$ , \*\*  $p < 0.01$  when high maternal mice were compared  
739 with control mice and  $^{**} p < 0.01$ ,  $^{***} p < 0.001$  when high maternal mice were compared with  
740 low maternal mice.



741

742 **Figure 7.** Estimation of the sensitivity and specificity of late-gestation GMC measures in the  
 743 entorhinal area (**A**) and accessory olfactory bulb (**B**) to predict postpartum maternal  
 744 performance.

745 Receiver operating characteristic (ROC) curves were estimated using a Wilson/Brown test with  
 746 a 95% confidence interval. Correlations were estimated using a Pearson correlation test. ROC  
 747 and correlation analyses were considered significant at  $p < 0.05$ .

# Label	Region of Interest	Hemisphere	T Value	p Value	x {mm}	y {mm}	z {mm}
712	Visceral area, layer 2/3	Left	2.3789	0.0094	-41.5	-3.5	-3.5
1842	Agranular insular area, dorsal part, layer 2/3	Left	3.9264	< 0.0001	-34.5	16.5	-8.5
652	Gustatory areas, layer 2/3	Left	3.4262	0.0004	-30.5	25.5	-4.5
2562	Cortical amygdalar area, posterior part, medial zone	Left	2.6591	0.0044	-23.5	-16.5	-18.5
3002	Olfactory tubercle	Left	4.2298	< 0.0001	-22.5	13.5	-23.5
2502	Piriform area	Left	3.6483	0.0002	-21.5	26.5	-14.5
3122	Medial amygdalar nucleus	Left	2.5052	0.0067	-21.5	-10.5	-11.5
2972	Caudoputamen	Left	2.5003	0.0068	-20.5	7.5	-6.5
3522	Lateral dorsal nucleus of thalamus	Left	2.3933	0.0090	-17.5	-4.5	4.5
292	Primary somatosensory area, lower limb, layer 2/3	Left	2.4134	0.0086	-16.5	4.5	23.5
1692	Orbital area, lateral part, layer 2/3	Left	2.4677	0.0074	-15.5	37.5	-0.5
2462	Anterior olfactory nucleus	Left	2.3608	0.0098	-11.5	33.5	-5.5
4132	Lateral hypothalamic area	Left	2.5217	0.0064	-10.5	-10.5	-18.5
2982	Nucleus accumbens	Left	2.3953	0.0090	-9.5	18.5	-15.5
3192	Diagonal band nucleus	Left	2.5835	0.0054	-5.5	14.5	-22.5
1731	Orbital area, medial part, layer 1	Right	2.5912	0.0053	1.5	37.5	0.5
2421	Main olfactory bulb	Right	3.7602	0.0001	2.5	35.5	-17.5
3861	Medial preoptic area	Right	2.6983	0.0040	6.5	11.5	-21.5
3971	Anterior hypothalamic nucleus	Right	2.4173	0.0085	8.5	-0.5	-20.5
4201	Tuberal nucleus	Right	2.4250	0.0083	8.5	-3.5	-20.5
4131	Lateral hypothalamic area	Right	3.3026	0.0006	11.5	-10.5	-16.5
11	Frontal pole, layer 1	Right	2.5614	0.0058	12.5	41.5	5.5
4141	Lateral preoptic area	Right	2.5685	0.0057	12.5	5.5	-18.5
2461	Anterior olfactory nucleus	Right	2.4144	0.0086	14.5	35.5	-7.5
2631	Dentate gyrus, molecular layer	Right	2.4871	0.0071	14.5	-16.5	12.5
3121	Medial amygdalar nucleus	Right	2.6129	0.0050	21.5	-10.5	-11.5
3001	Olfactory tubercle	Right	2.3745	0.0095	22.5	10.5	-24.5
1841	Agranular insular area, dorsal part, layer 2/3	Right	3.0066	0.0016	23.5	32.5	-2.5
2501	Piriform area	Right	2.9740	0.0018	26.5	24.5	-12.5
2971	Caudoputamen	Right	2.7880	0.0031	27.5	-7.5	-5.5
621	Supplemental somatosensory area, layer 6a	Right	2.4045	0.0088	29.5	8.5	2.5
591	Supplemental somatosensory area, layer 2/3	Right	2.5642	0.0057	36.5	16.5	-0.5

749

750 **Table S1.** Local variation in gray matter concentration between control and parous mice at the  
751 end of the gestation period. SPM flexible factorial analysis revealed an interaction between the  
752 control and parous groups at the late gestation time point.

# Label	Region of Interest	Hemisphere	T Value	p Value	x {mm}	y {mm}	z {mm}
712	Visceral area, layer 2/3	Left	4.0474	< 0.0001	-41.5	-3.5	-3.5
592	Supplemental somatosensory area, layer 2/3	Left	4.2243	< 0.0001	-40.5	6.5	-2.5
1842	Agranular insular area, dorsal part, layer 2/3	Left	3.9710	< 0.0001	-34.5	16.5	-8.5
352	Primary somatosensory area, mouth, layer 2/3	Left	1.9021	0.0293	-31.5	22.5	5.5
2972	Caudoputamen	Left	1.8455	0.0331	-31.5	-8.5	-0.5
342	Primary somatosensory area, mouth, layer 1	Left	1.7124	0.0437	-30.5	23.5	6.5
72	Primary motor area, layer 2/3	Left	1.7423	0.0411	-29.5	27.5	-0.5
232	Primary somatosensory area, barrel field, layer 2/3	Left	2.0289	0.0220	-27.5	6.5	18.5
532	Primary somatosensory area, unassigned, layer 2/3	Left	1.7753	0.0384	-27.5	11.5	16.5
2812	Subiculum	Left	3.0917	0.0012	-25.5	-24.5	10.5
2642	Dentate gyrus, polymorph layer	Left	1.7318	0.0420	-20.5	-23.5	-9.5
4092	Ventral premammillary nucleus	Left	2.3287	0.0107	-8.5	-14.5	-18.5
5522	Medial vestibular nucleus	Left	1.9545	0.0261	-5.5	-47.5	1.5
4442	Superior colliculus, motor related, intermediate gray layer	Left	2.9857	0.0017	-2.5	-14.5	13.5
2411	Olfactory areas	Right	2.0350	0.0217	0.5	23.5	-11.5
4031	Medial preoptic area	Right	1.6858	0.0461	5.5	-10.5	-19.5
2421	Main olfactory bulb	Right	2.4342	0.0081	2.5	34.5	-17.5
4541	Olivary pretectal nucleus	Right	2.6632	0.0044	6.5	-12.5	11.5
3211	Bed nuclei of the stria terminalis	Right	1.7760	0.0383	10.5	8.5	-6.5
4131	Lateral hypothalamic area	Right	2.0659	0.0202	11.5	-9.5	-17.5
4211	Zona incerta	Right	1.9015	0.0293	11.5	-8.5	-11.5
2791	Postsubiculum	Right	3.0783	0.0013	15.5	-18.5	12.5
3121	Medial amygdalar nucleus	Right	1.8183	0.0351	16.5	-10.5	-16.5
2561	Cortical amygdalar area, posterior part, medial zone	Right	3.5177	0.0003	22.5	-15.5	-19.5
401	Primary somatosensory area, upper limb, layer 1	Right	1.7139	0.0435	24.5	9.5	19.5
531	Primary somatosensory area, unassigned, layer 2/3	Right	1.7406	0.0412	26.5	9.5	18.5
61	Primary motor area, layer 1	Right	1.7743	0.0385	27.5	27.5	7.5
221	Primary somatosensory area, barrel field, layer 1	Right	2.2903	0.0118	27.5	5.5	19.5
2731	Entorhinal area, medial part, dorsal zone, layer 1	Right	1.9890	0.0241	27.5	-32.5	-1.5
231	Primary somatosensory area, barrel field, layer 2/3	Right	1.8671	0.0316	29.5	7.5	17.5
2571	Piriform-amygdalar area	Right	3.3855	0.0005	29.5	-6.5	-24.5
351	Primary somatosensory area, mouth, layer 2/3	Right	1.9950	0.0238	32.5	14.5	11.5
171	Primary somatosensory area, nose, layer 2/3	Right	1.8466	0.0330	33.5	12.5	11.5
2501	Piriform area	Right	3.4453	0.0004	36.5	-15.5	-17.5

753

754 **Table S2.** Local variation in gray matter concentration between control and parous mice at the  
755 beginning of the lactation period. SPM flexible factorial analysis revealed an interaction  
756 between the control and parous groups at the early lactation time point.

# Label	Region of Interest	Hemisphere	T Value	p Value	x {mm}	y {mm}	z {mm}
712	Visceral area, layer 2/3	Left	2.1741	0.01566	-41.5	0.5	-2.5
2812	Subiculum	Left	2.0845	0.01938	-28.5	-24.5	9.5
2972	Caudoputamen	Left	2.8735	0.00238	-28.5	-7.5	-3.5
2502	Piriform area	Left	2.3017	0.01143	-27.5	16.5	-16.5
2562	Cortical amygdalar area, posterior part, medial zone	Left	2.2071	0.01445	-23.5	-17.5	-17.5
2992	Fundus of striatum	Left	2.0065	0.0232	-20.5	8.5	-17.5
4442	Superior colliculus, motor related, intermediate gray layer	Left	1.9022	0.02927	-16.5	-21.5	10.5
2142	Anterior visual area, layer 2/3	Left	1.7105	0.04382	-13.5	-0.5	25.5
4082	Dorsal preamillary nucleus	Left	2.6229	0.00488	-5.5	-14.5	-15.5
3011	Lateral septal nucleus, caudal (caudodorsal) part	Right	2.2155	0.01416	4.5	8.5	7.5
3861	Medial preoptic area	Right	2.8305	0.0027	6.5	11.5	-21.5
3211	Bed nuclei of the stria terminalis	Right	1.7490	0.04052	7.5	14.5	-12.5
4131	Lateral hypothalamic area	Right	1.7901	0.03721	11.5	-6.5	-17.5
2621	Field CA3	Right	2.6408	0.00465	21.5	-18.5	-6.5
5161	Dorsal cochlear nucleus	Right	1.7477	0.04063	23.5	-43.5	-4.5
2561	Cortical amygdalar area, posterior part, medial zone	Right	1.8753	0.03104	24.5	-18.5	-17.5
2731	Entorhinal area, medial part, dorsal zone, layer 1	Right	1.9285	0.02763	27.5	-32.5	-1.5
2971	Caudoputamen	Right	2.8706	0.0024	30.5	-8.5	-1.5
701	Visceral area, layer 1	Right	1.8073	0.03589	41.5	3.5	-3.5

757

758 **Table S3.** Local variation in gray matter concentration between control and parous mice at the  
759 end of the lactation period. SPM flexible factorial analysis revealed an interaction between the  
760 control and parous groups at the late lactation time point.

# Label	Region of Interest	Hemisphere	T Value	p Value	x {mm}	y {mm}	z {mm}
992	Ventral auditory area, layer 6b	Left	2.4578	0.0084	-36.5	-15.5	5.5
2292	Temporal association areas, layer 6a	Left	2.7134	0.0043	-36.5	-24.5	8.5
242	Primary somatosensory area, barrel field, layer 4	Left	2.4559	0.0084	-33.5	0.5	12.5
2752	Entorhinal area, medial part, dorsal zone, layer 3	Left	3.7707	0.0002	-30.5	-29.5	-9.5
2812	Subiculum	Left	2.6370	0.0053	-29.5	-23.5	10.5
2212	Rostrolateral visual area, layer 4	Left	2.7190	0.0043	-23.5	-7.5	22.5
2622	Field CA3	Left	4.2394	0.0000	-21.5	-18.5	-6.5
4362	Substantia nigra, reticular part	Left	2.4952	0.0076	-17.5	-23.5	-5.5
72	Primary motor area, layer 2/3	Left	2.5921	0.0060	-12.5	13.5	20.5
2162	Retrosplenial area, dorsal part, layer 6a	Left	3.1820	0.0012	-11.5	-0.5	23.5
4132	Lateral hypothalamic area	Left	3.0784	0.0016	-11.5	-6.5	-17.5
2462	Anterior olfactory nucleus	Left	4.0594	0.0001	-10.5	31.5	-12.5
4212	Zona incerta	Left	3.0013	0.0020	-9.5	-10.5	-10.5
3862	Medial preoptic area	Left	2.6620	0.0050	-8.5	4.5	-20.5
4412	Superior colliculus, motor related, deep gray layer	Left	2.8740	0.0028	-8.5	-23.5	16.5
4012	Medial mammillary nucleus, medial part	Left	2.4376	0.0088	-4.5	-16.5	-16.5
4112	Ventromedial hypothalamic nucleus	Left	2.5173	0.0072	-3.5	-6.5	-22.5
4272	Superior colliculus, zonal layer	Left	2.8049	0.0034	-2.5	-14.5	17.5
4052	Tuberomammillary nucleus, dorsal part	Left	2.4993	0.0076	-1.5	-15.5	-19.5
4441	Superior colliculus, motor related, intermediate gray layer	Right	2.5749	0.0062	0.5	-26.5	19.5
4451	Periaqueductal gray	Right	2.4815	0.0079	3.5	-32.5	13.5
2651	Dentate gyrus, granule cell layer	Right	2.7718	0.0037	7.5	-7.5	10.5
4111	Ventromedial hypothalamic nucleus	Right	2.6915	0.0046	7.5	-6.5	-21.5
4431	Superior colliculus, motor related, intermediate white layer	Right	2.4866	0.0078	9.5	-28.5	18.5
2421	Main olfactory bulb	Right	3.9879	0.0001	10.5	38.5	-8.5
1071	Anteromedial visual area, layer 2/3	Right	4.0275	0.0001	12.5	-4.5	25.5
2971	Caudoputamen	Right	2.4763	0.0080	16.5	10.5	-7.5
2411	Olfactory areas	Right	3.9513	0.0001	17.5	30.5	-7.5
2621	Field CA3	Right	3.7785	0.0002	25.5	-17.5	-8.5
2811	Subiculum	Right	2.4734	0.0081	25.5	-23.5	11.5
1241	Posterolateral visual area, layer 1	Right	2.5546	0.0066	27.5	-31.5	19.5
2741	Entorhinal area, medial part, dorsal zone, layer 2	Right	4.0416	0.0001	29.5	-31.5	-8.5

761

762 **Table S4.** Local variation in gray matter concentration between low maternal behavior parous  
763 mice and high maternal behavior parous mice at the end of the gestation period. SPM flexible  
764 factorial analysis revealed an interaction between the low *versus* high maternal behavior groups  
765 at the late gestation time point.

# Label	Region of Interest	Hemisphere	T Value	p Value	x {mm}	y {mm}	z {mm}
2732	Entorhinal area, medial part, dorsal zone, layer 1	Left	2.5882	0.0060	-28.5	-33.5	1.5
2632	Dentate gyrus, molecular layer	Left	2.5173	0.0072	-20.5	-16.5	6.5
412	Primary somatosensory area, upper limb, layer 2/3	Left	3.1161	0.0014	-19.5	14.5	18.5
2602	Field CA1	Left	2.5276	0.0070	-19.5	-11.5	17.5
122	Secondary motor area, layer 2/3	Left	2.8890	0.0027	-15.5	24.5	15.5
2422	Main olfactory bulb	Left	3.5084	0.0004	-8.5	45.5	6.5
3652	Parafascicular nucleus	Left	3.0525	0.0017	-3.5	-12.5	-1.5
2672	Induseum griseum	Left	2.4662	0.0082	-1.5	19.5	5.5
1482	Anterior cingulate area, dorsal part, layer 1	Left	2.4675	0.0082	-0.5	21.5	14.5
2082	Retrosplenial area, ventral part, layer 1	Left	2.3913	0.0099	-0.5	-3.5	23.5
2421	Main olfactory bulb	Right	2.7201	0.0043	2.5	43.5	-14.5
3651	Parafascicular nucleus	Right	2.9370	0.0023	6.5	-12.5	0.5
2411	Olfactory areas	Right	3.2967	0.0008	8.5	42.5	4.5
2601	Field CA1	Right	3.6131	0.0003	18.5	-9.5	17.5
381	Primary somatosensory area, mouth, layer 6a	Right	3.1451	0.0013	24.5	14.5	5.5
2821	Prosubiculum	Right	2.9853	0.0020	24.5	-19.5	14.5
2691	Entorhinal area, lateral part, layer 2	Right	3.0830	0.0015	38.5	-29.5	-5.5

766

767 **Table S5.** Local variation in gray matter concentration between low maternal behavior parous  
768 mice and high maternal behavior parous mice at the beginning of the lactation period. SPM  
769 flexible factorial analysis revealed an interaction between the low *versus* high maternal  
770 behavior groups at the early lactation time point.